frontiers | Frontiers in Astronomy and Space Sciences

TYPE Original Research
PUBLISHED 24 April 2023
DOI 10.3389/fspas.2023.1092850

OPEN ACCESS

EDITED BY
Joseph Huba,
Syntek Technologies, United States

REVIEWED BY
Shun-Rong Zhang,
Haystack Observatory, United States
Bapan Paul,
Vivekananda B.Ed and D.El.Ed College, India

*CORRESPONDENCE
K. A. Berényi,
berenyi.kitti@epss.hu

RECEIVED 08 November 2022
ACCEPTED 11 April 2023
PUBLISHED 24 April 2023

CITATION
Berényi KA, Heilig B, Urbář J, Kouba D, Kis Á and Barta V (2023), Comprehensive analysis of the ionospheric response to the largest geomagnetic storms from solar cycle 24 over Europe.
Front. Astron. Space Sci. 10:1092850.
doi: 10.3389/fspas.2023.1092850

Comprehensive analysis of the ionospheric response to the largest geomagnetic storms from solar cycle 24 over Europe

K. A. Berényi[1,2,3]*, B. Heilig[3,4], J. Urbář[5], D. Kouba[5], Á. Kis[3] and V. Barta[3]

[1]ELKH-ELTE Space Research Group, Budapest, Hungary, [2]Doctoral School of Environmental Sciences, ELTE Eötvös Loránd University, Budapest, Hungary, [3]Institute of Earth Physics and Space Science, Sopron, Hungary, [4]Space Research Group, Eötvös Loránd University, Budapest, Hungary, [5]Institute of Atmospheric Physics CAS, Prague, Czechia

A multi-instrumental analysis of the meridional ionospheric response is presented over Europe during the two largest ICME-driven geomagnetic storms of solar cycle #24 maximum. Data from 5 European digisonde stations, ground-based Global Navigation Satellite System, Total Electron Content (GNSS TEC), the ratio of the TEC difference (rTEC), as well as Swarm and Thermosphere, Ionosphere, Mesosphere, Energetics and Dynamics (TIMED) satellite observations have been used for the investigation of selected intervals (11–17 November, 2012, and 16–25 March, 2015). The storm evolution is monitored by digisonde foF2 critical frequency (related to the maximum electron density of F2-layer) and GNSS TEC data. Moreover, Global Ultraviolet Imager (GUVI) measurements from the TIMED satellite are used to investigate the changes in the thermospheric O/N_2 ratio. Our main focus was on the main phase of the geomagnetic storms, when during the nighttime hours extremely depleted plasma was detected. The extreme depletion is observed in foF2, TEC and rTEC, which is found to be directly connected to the equatorward motion of the midlatitude ionospheric trough (MIT) on the nightside. We demonstrate a method (beside the existing ones) which allows the monitoring of the storm-time evolution of the disturbances (e.g., MIT, SAPS, SED) in the thermosphere-ionosphere-plasmasphere system by the combined analysis of the worldwide digisonde system data (with the drift measurements and the ionospheric layer parameters with 5–15 min cadence), with rTEC and GNSS TEC data, and with the satellite data like Swarm, TIMED/GUVI.

KEYWORDS

geomagnetic storms, space weather, ionosphere, ionospheric storm, midlatitude ionospheric trough, GNSS TEC, ionosphere-plasmasphere coupling, Swarm observations

1 Introduction

The physical processes of the Earth's plasma environment responsible for the perturbations of the system and the exact mechanisms of action of solar events affecting the near-Earth space have been of interest to researchers for decades. The most remarkable disturbing solar activity events are interplanetary coronal mass ejections (ICMEs) and high-speed solar wind streams (HSSWS)/corotating interaction regions (CIRs). When they collide with the Earth's magnetic field, they trigger geomagnetic storms. The two types of geomagnetic storms have different time courses and result in different magnitudes of

perturbations. Besides there are several processes that have to be taken into consideration during the examination of the mid- and low latitude ionosphere, as follows: photo-production, chemical loss, and transport by thermal expansion, neutral winds, waves, tides and electric fields of internal and external origin (Mendillo and Narvaez, 2009). In addition, several other influencing factors must be taken into consideration, such as: geomagnetic storm size, local time (LT) of the sudden storm commencement (SSC), time of the day, season, geomagnetic latitude and longitude (Immel and Mannucci, 2013; Mendillo and Narvaez, 2010; Mendillo and Narvaez, 2009).

Within the Earth's plasma environment (ionosphere, plasmasphere, outer magnetosphere), all regions are closely related to each other. In the presence of an external forcing (e.g., ICME or CIR/HSSWS), perturbations can be observed in each plasma layer. The F-layer of the ionosphere has the highest electron density, so electron density changes are the most pronounced there. The electric fields generated during geomagnetically disturbed periods (e.g., prompt penetration of magnetospheric convection electric field-PPEF and disturbance dynamo electric field-DDEF) map along geomagnetic field lines through all these regions and can interact with all of them (see e.g., Nava et al., 2016). The Earth's plasma environment is a very complex, tightly coupled system, and the effects cannot be studied and explained in their entirety if we do not consider them as part of the system.

Geomagnetic storms generate so-called ionospheric storms, which have similar evolution and phases to those of geomagnetic storms, but with a faster procession. Ionospheric storms have already been studied using several types of observations of the F2-layer: ionosonde data of the maximum electron density (NmF2); measurements of the total electron content; incoherent scatter radar measurements of electron and ion densities, temperatures and plasma dynamics; satellite measurements of ionospheric/thermospheric parameters along their orbits (see e.g., Kane and Makarevich, 2010). Comprehensive reviews of storm effects in NmF2 and TEC have been given by Prölss (1995) and Mendillo (2006), for incoherent scatter radar results by Buonsanto (1999), and for *in-situ* satellite data by Prölss and Zahn (1974).

In early studies, two different phases of ionospheric storms were distinguished: positive ionospheric storm phase, when the electron density is increased, and negative ionospheric storm phase, when the electron density is decreased with respect to its expected value. Earlier studies during the past few decades have already found clear and unambiguous patterns in the ionosphere during geomagnetic storms, see for example, the great reviews of Sato (1957), Matsushita (1959), Prölss (1995), Danilov (2013) (for ionosonde data) and Mendillo (2006) (for TEC data).

The various perturbations in the midlatitude ionosphere during geomagnetic storms can be linked to various processes detailed below. For case studies of ionospheric storm effects, it is necessary to determine the key drivers of the actual events.

(1) During geomagnetic storms, the Joule dissipation of currents and the absorption of precipitating particles in the auroral region of the lower thermosphere (100–140 km) are the cause of the so called auroral heating of the thermosphere (Prölss, 1995; Danilov, 2013). The location of both the precipitation boundary and the auroral currents depends on the geomagnetic activity. For intense storms, it could be found below L = 2.5 (Mendillo and Narvaez, 2009). There are two major consequences of high-latitude heating: composition changes (specifically, decrease in the O/N_2 ratio) and the intensification of equatorward winds that can carry the composition change toward lower latitudes (Buonsanto, 1999). Both processes contribute to the formation of long-duration negative storm phases. The electron density near the F2-layer maximum is, approximately, directly proportional to the O/N_2 ratio (Rishbeth and Barron, 1960; Pirog, 2006). This means, if other conditions are unchanged (constant pressure), we should detect depletion in electron density (negative phase) in all regions where O/N_2 ratio has been decreased at F2-layer heights (Danilov, 2013). Under geomagnetic storm conditions this so-called compositional disturbance zone at F2-layer heights reaches lower latitudes because of the intensified heating induced equatorward meridional winds. Negative phase is most common in the summer hemisphere (both day and night) due to the seasonal variation of the background thermospheric wind circulation, but during intense geomagnetic storms it can be detected even in winter months. It favors the postmidnight and morning sectors, because then the background and the storm-induced circulation coincide and add up and therefore can reach much lower latitudes (Prölss, 1995; Buonsanto, 1999; Danilov, 2013). This equatorward expansion of the negative phase has about 50–300 m/s velocity (Danilov and Belik, 1991). Besides the O/N_2 ratio depletion, the increased temperature of the heated thermospheric gas itself is an important factor in forming a negative storm phase in the ionosphere (Mikhailov and Foster, 1997). The increase in temperature leads to an increase in the recombination coefficient causing a further decrease in electron density (see Mikhailov et al., 1995). Previous studies concluded that at high and middle latitudes this negative phase type occurs more often, and has much more dangerous effect on HF propagation (Danilov, 2013).

Long-duration positive ionospheric storm phase can be generated by the enhanced storm-induced equatorward meridional winds because they cause the downwelling of the neutral atomic oxygen and the uplifting of the F-layer along the magnetic field lines due to wind induced vertical ExB drift (Prölss, 1995; Danilov, 2013). A similar drift can also be caused by an increase in E-fields of other origin (e.g., from the magnetosphere) (Danilov, 2013). As the loss-rate decreases with altitude, the density increases.

(2) The ionospheric F- region plasma is the base of the plasmasphere (Mendillo et al., 1974), i.e., the plasmasphere is filled from the dayside ionosphere and empties into the nightside F-region through diffusion along the geomagnetic field lines. Under quiet conditions the midlatitude region maps into the plasmasphere corotating with the Earth. During storms the footprint of the plasmapause (PP) often moves to midlatitudes, especially after sunset (Mendillo and Narvaez, 2009) as the plasmapause moves inward due to the increased geomagnetic activity, while the plasmasphere can still remain conjugated with the midlatitude ionosphere during

daytime hours. Thus, from local noon to dusk the dynamical plasmaspheric processes may contribute to daytime positive-phase ionospheric storms (Lanzerotti et al., 1975), which is followed after sunset by a sharp transition to a depleted state beyond the footprint of the plasmapause (Mendillo et al., 1974). After sunset, both the above discussed dynamics and chemistry cause the onset of a negative phase.

(3) During intense geomagnetic storm events, mainly in the main phase, at night, a drastic "peeling off" of the magnetospheric plasma can be seen, and the ionospheric projection of the PP can penetrate into the midlatitude region also on the dayside. In such a case, an all-day negative phase storm is expected. Based on earlier studies like Heilig et al. (2022), it is stated that the ionospheric footprint of the PP is tightly coupled to the minimum of the midlatitude (main) ionospheric trough (MIT). The poleward edge of the MIT in the evening sector has been observed to coincide with the equatorward boundary of the soft electron precipitation, and the precipitation has therefore been proposed as a major source of electrons building up the poleward wall of the MIT in the evening sector (Turunen and Liszka, 1972; Rodger et al., 1986; Voiculescu et al., 2010). During the night the ionospheric F-layer on the equatorward side of the plasmapause is maintained by the plasmasphere, but not on the global convection dominated poleward side (Schunk and Banks, 1975). Consequently, an MIT minimum could be bounded by a plasmasphere-maintained and the precipitation-maintained ionosphere. The minimum could be sharpened by storm-time developed subauroral polarization streams (SAPS) due to SAPS E-field, and by plasma heating (frictional heating by the drifting plasma) and its consequences (Rodger et al., 1992; Horváth and Lovell, 2016), and by enhancing recombination due to molecular composition changes by neutral winds or diffusion from the aurora oval = composition disturbance zone (1) (Schunk and Banks, 1975).

MIT is a longitudinally elongated and latitudinally restricted region of depleted plasma in the ionosphere (He et al., 2011). Its typical latitudinal extent (width) is 5°–10° (Voiculescu et al., 2010), 10°–15° (Liu and Xiong, 2020), but it can be as wide as 20°. MIT is typically found somewhere between 55° and 75° geographic latitude depending on the geomagnetic activity and MLT (e.g., Whalen, 1989; Werner and Prölss, 1997; Voiculescu et al., 2006; Deminov and Shubin, 2018; Karpachev et al., 2019; Aa et al., 2020; Liu and Xiong, 2020). However, as we will show, in severely disturbed cases it can move even further equatorward. MIT typically occurs in the dark hemisphere, thus, it is most regularly observed during winter months and equinoxes, while in summer, it is mainly restricted to the midnight sector (Rodger et al., 1992; Voiculescu et al., 2006).

Over the years, the general behavior of the ionosphere during storms has become well studied. However, each space weather event and the involved processes are unique, and in many cases the magnitude of the effects cannot yet be predicted. Consequently, case studies of extraordinary/high magnitude events are still important as they can deepen/refine our understanding of the extent of change that can be expected in the individual layers of the Earth's plasma in response to a geomagnetic storm. Furthermore, multi-instrumental comprehensive analysis of the thermosphere-ionosphere-plasmasphere coupling processes during individual geomagnetic storms are rare in the literature. Most studies are based on one or two types of observational data, however the effects cannot be studied separately since the Earth's plasma environment is a very complex, multiplied coupled system.

In this study our aim is to determine the exact connections between the thermosphere-ionosphere-plasmasphere system during two intense ICME-caused geomagnetic storm events. We analyzed the effects through a meridional chain of digisondes (foF2, h'F2 and drift data) across Europe (Northern Hemisphere) complemented by GNSS TEC, Swarm satellite observations of the topside electron density, electron temperature and PP location data, as well as O/N_2 ratio observations from TIMED satellite. Another aim is to identify the processes responsible for the extreme decrease during the night in the main phase of the geomagnetic storm. The rest of the paper is organized as follows. First, the utilized data and the applied methods are introduced. In Section 3 the observations are presented, followed by the discussion in Section 4. Finally, main conclusions are summarized in Section 5.

2 Data and method

In the present study our main focus is on the analysis of the effects in the ionospheric F2-layer during two intense ($Dst_{min} > -100$ nT) ICME related geomagnetic storms. The storms considered are from the winter/equinox of 2012 and 2015 (the maximum of #24 solar cycle), respectively, with the following characteristics: 11–17/11/2012 ($Dst_{min} = -108$ nT, $Kp_{max} = 6.33$) and 16–25/03/2015 ($Dst_{min} = -223$ nT, $Kp_{max} = 7.67$).

For the investigation, intervals covering all the pre-storm (24 h before the SSC), initial, main and recovery phase were selected. We used the geomagnetic Dst-index to identify the storm phases. A sudden sharp increase in the data is observed when an SSC occurs, this is followed by a major decrease in the data (main phase), and then a slower recovery lasting for several days. The magnitude of the storm itself is given by the minimum value of Dst. The AE-index (auroral electrojet index - mainly characterizing the polar region) increases as the substorm activity intensifies.

We analyzed individual events to see in detail the processes and to determine the key drivers of the geomagnetic storm generated ionospheric perturbations. Using the meridional station chain, the latitudinal evolution of the effects can be followed. With the digisonde drift measurements the directions of the associated plasma drifts can be determined. Using also satellite data, the thermospheric (with TIMED, GUVI measurements) and plasmaspheric (with Swarm, Langmuir probe measurements) processes can be linked to the perturbations observed in the ionosphere. The measurements and data utilized are listed below:

2.1 Solar and geomagnetic indices

During case studies we typically identify and characterize the storm events considering the magnitude of geomagnetic indices such as Kp, Dst and AE. The Kp index represents the geomagnetic activity of the midlatitudal regions, and it has logarithmic scale.

TABLE 1 In this table, we can see information about the used 5 digisonde stations. For the geomagnetic coordinates, International Geomagnetic Reference Field (IGRF-13)-model (for year 2015) based calculator was used.

	Name of the station	Station ID	Geomagnetic latitude (deg)	Geomagnetic longitude (deg)	Geographic latitude (deg)	Geographic longitude (deg)
High mid-latitude	Juliusruh	JR055	53.95° N	99.48°E	54.6° N	13.4° E
Middle latitude	Pruhonice	PQ052	49.32° N	98.61° E	50° N	14.6° E
	Sopron	SO148	46.67° N	99.75° E	47.63° N	16.72° E
Low mid-latitude	Rome	RO041	41.7° N	93.76° E	41.8° N	12.5° E
	Athens	AT138	36.17° N	103.33° E	38° N	23.5° E

The Dst index shows the intensity of the ring current and as we mentioned above are generally used to separate the geomagnetic storm's phases case to case. The AE index describe the evolution of the auroral electrojets, so it inform us about the processes at high latitudes.

2.2 Ionosonde data

A meridional ionosonde station chain across Europe was selected to represent the latitudinal changes. The following 5 stations were chosen for the analysis (from North to South): Juliusruh (JR), Pruhonice (PQ), Sopron (SO), Rome (RO), and Athens (AT). In Table 1, information on the ionosonde stations is given. LT = UT +1. Most of the stations are operating with a DPS-4D type of ionosonde, a digisonde. Only SO is an exception where a VISRC-2 type ionosonde operated until 2018, when the same DPS-4D type digisonde was installed also here (Bór et al., 2020). Old ionosonde/digisonde data has typically 30/15 min resolution, respectively, however, in some cases (like at Athens station) data are available at 5-min cadence.

During this investigation, two ionospheric parameters of the F2-layer were examined, namely, foF2, h'F2. The foF2 parameter represent the F2 layer critical frequency associated with the maximum plasma (electron) density of the F2 layer, while the h'F2 parameter reflects the changes in the virtual height of the layer. All digisonde data were manually checked and corrected with SAO Explorer. Besides, modern digital ionosondes provide also routine ionospheric drift measurements in addition to classical vertical ionospheric sounding (for more see the Supplementary Data section and Kouba et al., 2008; Kouba and Koucka Knizova, 2012; Kouba and Koucka Knizova, 2016). The ionospheric drift data for the selected storms of this study were manually processed for the PQ station. Nowadays, tens of digisondes worldwide measure ionospheric drifts routinely and store their data in Global Ionosphere Radio Observatory (GIRO).

Reference values were needed to determine the magnitude of the storm-time deviations from the nominal state. For this, we chose the 3 closest geomagnetically quiet days (QDs) preceding the storms investigated (8, 9, 10 November 2012 and 10, 13, 14 March 2015, respecti721vely) based on the International Q-days (QD) list, and averaged them. These reference values appear as green lines in Figure 3; Figure 4; Figure 5; Figure 6.

2.3 TEC data

GNSS TEC IONEX (IONosphere Map EXchange) maps data (http://ftp.aiub.unibe.ch/ionex/draft/ionex11.pdf) International GPS Service for Geodynamics (IGSG) with 2-hourly cadence were used to determine vertical TEC (vTEC) development in areas surrounding the respective digisondes, each map area of size 2.5 (latitude) x 5 (longitude) degrees.

For comparison, the National Institute of Information and Communications Technology (NICT) Ratio of the TEC difference (rTEC) global maps constructed using the RINEX files obtained from thousands of GNSS receivers all over the world were applied for the European region with a grid of 0.5 × 0.5° and smoothed with a 5 × 5 boxcar. The rTEC value was defined as the difference between the observed TEC and the monthly average quiet TEC value (mean of 10 geomagnetically quietest days), normalized by the average TEC.

2.4 TIMED satellite, global ultraviolet imager (GUVI) O/N_2 measurements

The TIMED satellite has been operating at 625 km altitude since December of 2001 and focuses its measurements to the appr. 60–180 km altitude range (neutral thermosphere and ionosphere) below the satellite (Christensen et al., 2003). TIMED is orbiting on a circular polar orbit with an inclination of 74.1° corresponding to 97.8 min period, which means that a global map of the measurements can be derived from 14.9 daily orbits.

GUVI measurements provide dayside O/N_2 composition (note that this is a column integrated value for an altitude range) and temperature profile of the Mesosphere and Lower Thermosphere/Ionosphere (MLTI) region, as well as the auroral energy inputs (Christensen et al., 2003; Crowley et al., 2006; http://guvitimed.jhuapl.edu/home_background).

2.5 Swarm satellite measurements

The three Swarm satellites were launched into a polar low-Earth orbit (LEO) in November 2013. The altitude of Swarm A

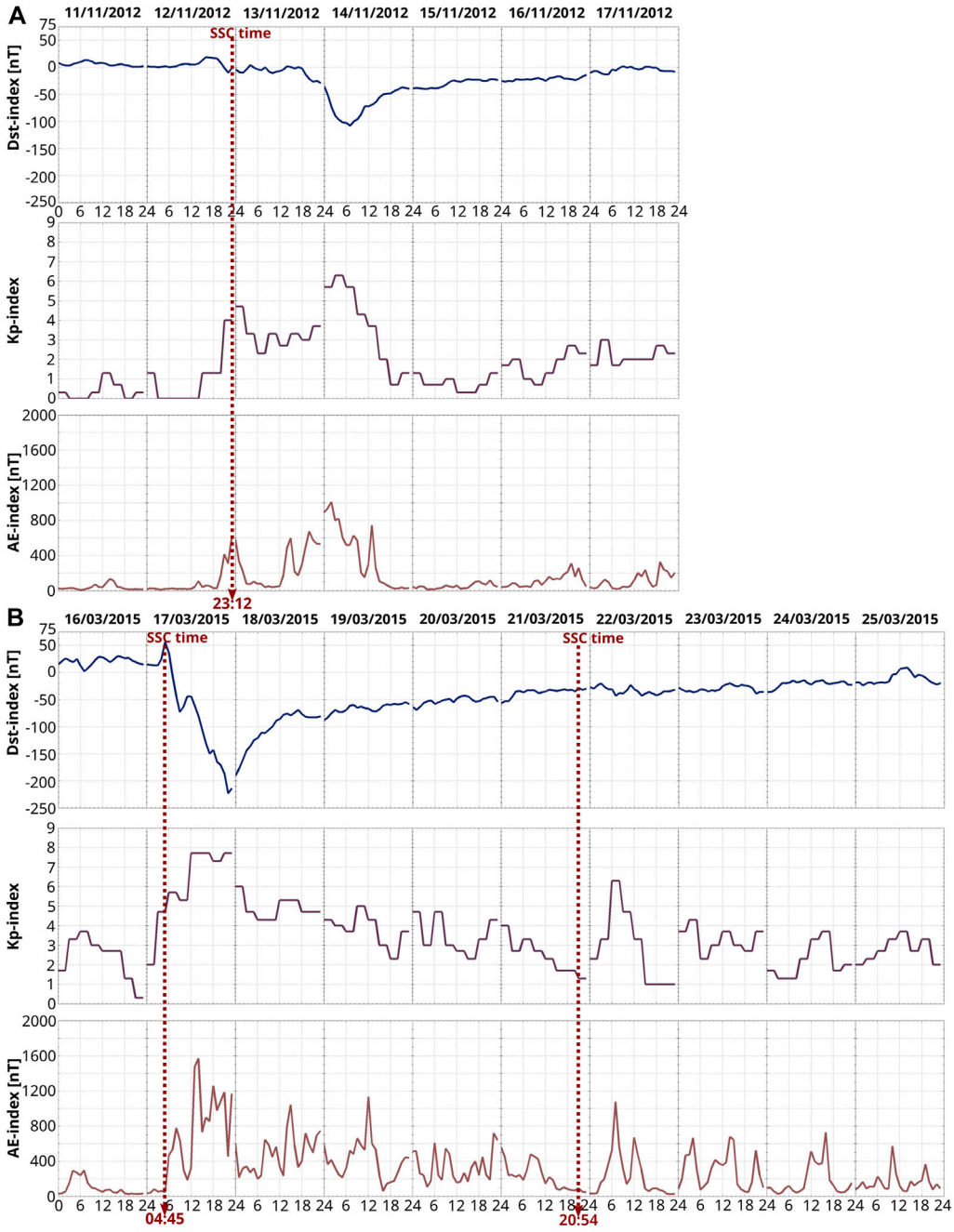

FIGURE 1
The geomagnetic Dst, Kp and AE indices are plotted for the 2012 November storm **(A)**, and for the 2015 March storm **(B)**. In the upper diagrams the daily variation of the Dst index is presented, in the middle panel the Kp index, while in the bottom the daily variation of the AE index is shown. The UT of the SSC was at 23:12 for the 2012 storm marked with a red dotted line. In the 2015 storm, the first storm commenced at UT 04:45, while the second SSC was at 20:54 (red dotted lines).

and C (flying side-by-side with ca. 1.5° longitudinal difference) was around 460 km in March 2015, while Swarm B was operating at around 520 km altitude, with a 91 min orbiting period. Swarm satellites provide *in-situ* measurements of the electron density and temperature observed by Langmuir probes, as well as the location of the MIT from which the footprint of the nightside plasmapause can be derived.

3 Observations

In our previous article (Berényi et al., 2018), the characteristics of the 2012 November and 2015 March storm were described in detail, the course of the storms was investigated in several aspects using data from the Sopron ionosonde station. In this article, we discuss the meridional evolution and characteristics of the two

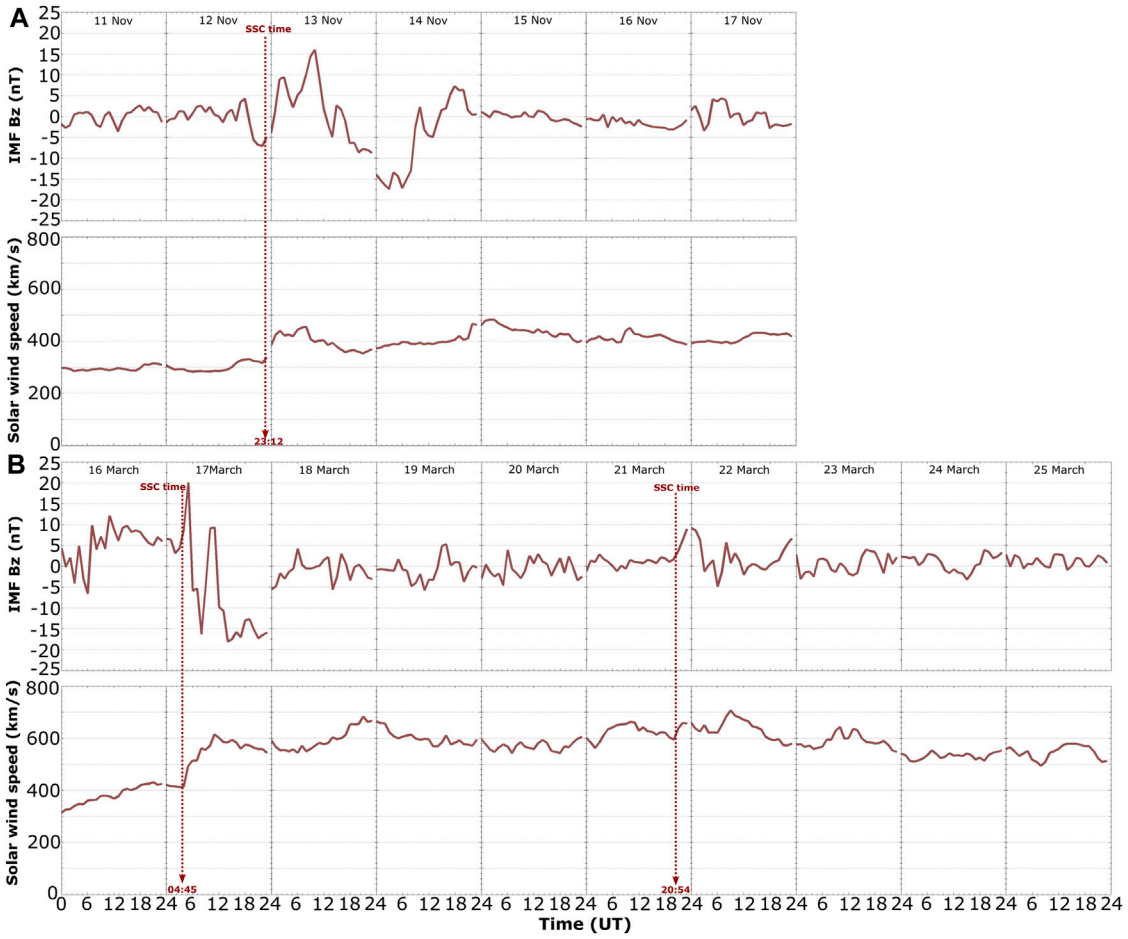

FIGURE 2
The interplanetary magnetic field (IMF) Bz component and the solar wind speed data can be seen for the two investigated storm intervals. **(A)** Is for the 2012 November, **(B)** is for the 2015 March storm. The SSC times are with red dotted lines (Supplementary Figure S1 is the same, except that it is with 1-min resolution).

investigated storms using several types of measurements, detailed in Section 2.

According to the ACE satellite data, in the case of storm from 2012 November, the geomagnetic disturbance started with two ICMEs shock arrivals at 22:16 UT on 12 November (source: SWPC PRF 1942, 19 November, 2012; https://izw1.caltech.edu/ACE/ASC/DATA/level3/icmetable2.htm). The storm started with a Sudden Storm Commencement (SSC) at 23:12 UT (00:12 LT) on 12 November On Figure 2A the evolution of the interplanetary magnetic field (IMF) Bz component and the solar wind (SW) speed data are plotted (1-min resolution is on Supplementary Figure S1A). During the SSC time, short southward turning of the Bz appeared which 1 h later turned northward and lasted until ca. 13 h. In the meanwhile the SW speed from 300 km/s after the SSC went up to 420 km/s and it oscillated around this value through the whole storm interval. Early on 14 November the storm reached its maximum magnitude (major storm), which was caused by a prolonged period of negative Bz (Figure 2A) from 8 h to 18 h, attributed to a combination of lingering ICME effects and a solar sector boundary crossing that occurred at approximately 02:45 UT. Right after that a negative polarity coronal hole associated high speed solar wind stream (HSSWS) arrived. The main phase of the geomagnetic storm started on 14 November (Dst_{min} = −108 nT, Kp_{max} = 6.33), this can be distinctly seen in Figure 1A in the evolution of the geomagnetic Dst, Kp and AE indices.

The 2015 March geomagnetic storm started with an SSC at 04:45 UT (05:45 LT) on 17 March, around equinox. The magnitude of this storm was (on day 17 March): Dst_{min} = −234 nT, Kp_{max} = 7.67 (see also Figure 1B). More information about this ICME generated geomagnetic storm can be found in the article of Wu et al. (2016). On Figure 2B the IMF Bz and SW speed values were displayed (1-min resolution is on Supplementary Figure S1B). The most significant episodes: right after the SSC the northward Bz turned southward around 7 UT, this followed by a northward turning around 10, then from noon until midnight a prolonged southward Bz can be observed. The SW speed values increased from an initial 400 km/s to 600 km/s around noon on17 March, and peaked at 700 km/s on the night of 18 March. On the days after the ICME the Earth was inside the flow of HSSWS (Nava et al., 2016). A subsequent geomagnetic

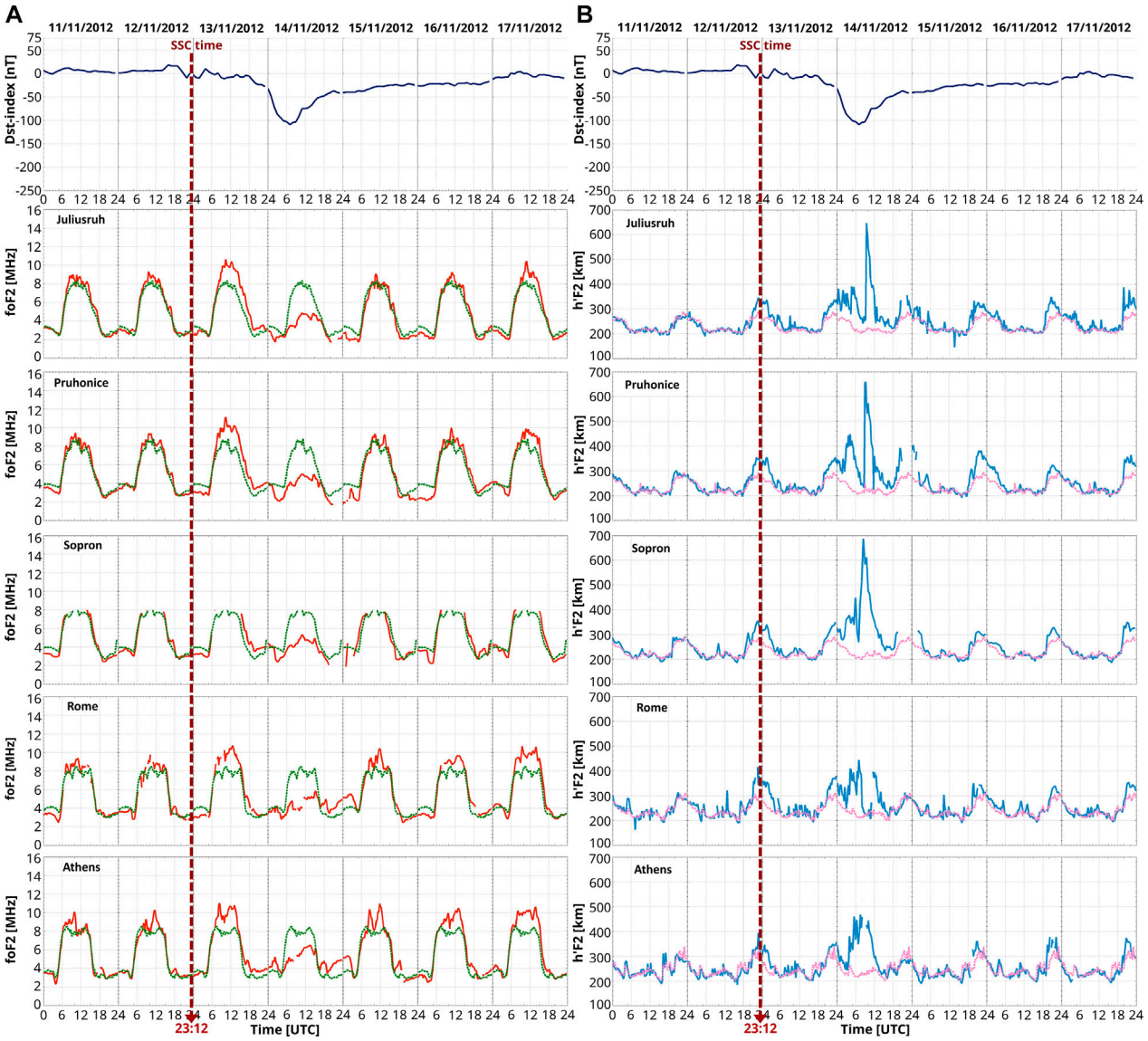

FIGURE 3
On the upper diagrams the Dst-index values and on the lower diagrams the storm-time foF2 (with red line, A)) and h'F2 (with light blue line, B)) with the reference foF2, h'F2 values of selected 3 quiet days [with dotted green **(A)** and pink line **(B)**] are portrayed for storm 2012 over the meridional station chain.

disturbance which is connected to a HSSWS (see Figure 1B) started at 20:54 UT on 21 March, which does not appear in the value of the Dst index, but is clearly visible in the Kp and AE index (see Figure 1B) (Nava et al., 2016). Several articles have been published in recent years about this storm, also known as St. Patrick's Day storm, which is the largest storm of the solar cycle 24 (e.g., Astafyeva et al., 2015; Cherniak and Zakharenkova, 2015; Zhang J.J. et al., 2015; Zhang S.R. et al., 2015; Li et al., 2016; Wu et al., 2016; Nayak et al., 2016; Nava et al., 2016; Kalita et al., 2016; Tulasi et al., 2016; Hairston et al., 2016; Jin et al., 2017; Polekh et al., 2017; Zhang S.R. et al., 2017a; Zhang S.R. et al., 2017b and references therein; Berényi et al., 2018; Huang et al., 2018; Habarulema et al., 2018; Kumar and Kumar, 2019; Ratovsky et al., 2019; Lu et al., 2020).

3.1 Digisonde data over Europe

The main results presented in the following were derived from ionosonde and digisonde measurements across a meridional station chain introduced in Section 2. In this section, the evolution of the ionospheric foF2, h'F2 is shown. Using data of European ionosonde stations for comparison, our primary goal is to check whether the ionosonde recorded effects at Sopron station (Berényi et al., 2018) were local or regional/global. Furthermore, we would like to illustrate how an ionospheric storm develops from North to South, along a geomagnetic meridian. Through this demonstration, the turning point of the ionospheric phase development can be determined (see Buonsanto, 1999; Kane, 2005). In a general case, over the auroral region a negative

ionospheric storm phase can be observed, while over lower latitudes (closer to the equator) this turns into a positive phase (the exact latitude of the phase reversal depends e.g., on the season, LT, the strength of the geomagnetic storm, meridional winds, etc.). First, we present ionosonde observations for the extended 2012 and 2015 storm periods.

3.1.1 Geomagnetic storm 11-17/11/2012

The first phenomenon known from previous studies, which can appear in foF2 even 24 h before the SSC during the daytime hours, is called the pre-storm enhancement (Kane, 2005; Burešová and Laštovička, 2007; Danilov, 2013). This can be also observed in all the 5 digisonde stations, though it is not very well pronounced (see Figure 3). On the contrary, during the night on 11/12 November all station data show negative phase, except for AT where no change can be detected.

On the right panel of Figure 3, the virtual height of the F2-layer (h'F2) is presented, not any significant daytime change at any station can be seen on 12 November, however a quite significant increase can be observed during the night starting at 21:00 UT, just before the SSC.

Right after the SSC at 23:12 UT, an increase in electron density (foF2 parameter) can be seen during that night and then during the day on 13 November at all stations. This is the main phase of the ionospheric storm, but the geomagnetic storm main phase starts only later on the following day. At the beginning of the following night, still positive phase at all stations can be seen, but around midnight it turns negative at JR, PQ and SO. Besides, a significant increase in h'F2 appears already around 20:00 UT which lasts even throughout the next day (14 November).

During the daytime hours in the main phase of the geomagnetic storm (14 November) a negative ionospheric storm phase was observed at all stations. In the meantime, the F2 layer was extremely uplifted, up to 680 km at stations SO, PQ and JR (Figure 3, right panel). In this case, we observe a negative ionospheric storm phase during a relatively weak (i.e., closer to moderate) geomagnetic storm. This event can be considered as an atypical storm, since the main phase of the geomagnetic storm is delayed by 1 day. In a regular storm, the main phase typically starts with a significant positive or negative ionospheric storm phase within a few hours after the SSC.

Note. during this storm the ionosonde at Sopron provided observations only up to 8 MHz, but the negative ionospheric response during the main phase of the geomagnetic storm clearly shows up.

This storm can be identified as a Regular Positive Phase (RPP) storm type following the nomenclature introduced by Mendillo and Narvaez (2010) according to the meridional evolution of foF2. Their classification is based on the local time of the SSC, which was in this case around midnight (00:12 LT) on 13 November The significant increase of foF2 (electron density) lasted from around 10–11:00 to 20:00 LT at all stations, and this positive phase was followed by a negative phase on 14 November.

In Figure 3 during the main phase of the geomagnetic storm at night hours (18:00–02:30 UT), a negative ionospheric storm phase can be observed at the SO, PQ and JR stations. The electron density decreased below the detectability level (disappeared from the ionograms) at these stations. Along with this electron density drop, the virtual height of the F2-layer increased up to 400 km (from the 250–280 km QD value) before the observed fade-out (see Figures 1, 3, as well as the Supplementary Table S1). On the contrary, at RO and AT stations, a significant increase of the foF2 parameter (electron density) with respect to the reference days could be seen during the night. Furthermore, the h'F2 was not as increased at RO and AT during this period as at the other stations. In Supplementary Table S1 the exact time and duration of the fade-outs, the start time of the decrease/increase and the minimum/maximum values are tabulated (the foF2 value in MHz).

From 15 November, during the early recovery phase, a so-called early recovery phase enhancement effect was detected in foF2 at stations AT, RO, SO and PQ (see Figure 3). This effect with increased electron density around noon lasts 3-day long, most significantly at Rome and Athens station, but observable at the other stations, too (see Figure 3). On the other hand, during the nighttime hours of 15 November a negative phase appears at all stations, while on 16 November only JR and PQ are negative, SO does not show any clear trend, and RO and AT are positive.

During the recovery phase, no deviation from the reference quiet time h'F2 was seen during daytime, however there was a quite significant increase during the night, first of all at the PQ station, but less pronounced also at SO and JR.

3.1.2 Geomagnetic storm 16-25/03/2015

The evolution of the 2015 March geomagnetic storm started on day 17th. The local time of the SSC was at 05:45 on 17 March (these are marked with a red dotted line in Figure 4). After the SSC, during the main phase of the ionospheric and geomagnetic storm, a positive phase of the ionospheric storm started at all stations. These kinds of storms are called Regular Positive Phase (RPP) storms because in the main phase of the storm, the electron density (foF2) increases, with no delay (Mendillo and Narvaez, 2010). At the same time, there is also a significant increase in height of F2-layer (h'F2) during daylight hours at all stations, but much less pronounced at RO and AT (see the right panel of Figure 4).

The most significant increase in the virtual height of the F2-layer occurred from around 20:00 UT (21 LT) on 17 March. The highest peak of the h'F2 parameter was observed at Pruhonice at 587.6 km at 22:45 UT. This main phase pattern in h'F2 parameter lasts until 21 March, and appears significant at SO, PQ and JR stations (see Figure 4).

Besides, during the evening/night on 17/18 March, a sharp decrease in the electron density was observed, the start of the negative phase began at noon at JR and it occurred later and later with decreasing latitude. The depletion was the most pronounced at PQ, SO and RO (see Figure 4 and Supplementary Table S2). The electron density decreased below the detectability level (disappeared from the ionograms) for a short period at RO and SO station. In Supplementary Table S2 the exact time and duration of the fade-outs, the start time of the negative phase and the time of the observed minimum value are tabulated. Along with this electron density drop, the virtual height of the F2-layer increased up to 483 km (from the 250–280 km QD value) before the fade-out at Sopron (see Figure 4).

Depletions in the foF2 parameter value (negative phase) compared to the main phase value can be observed on the next

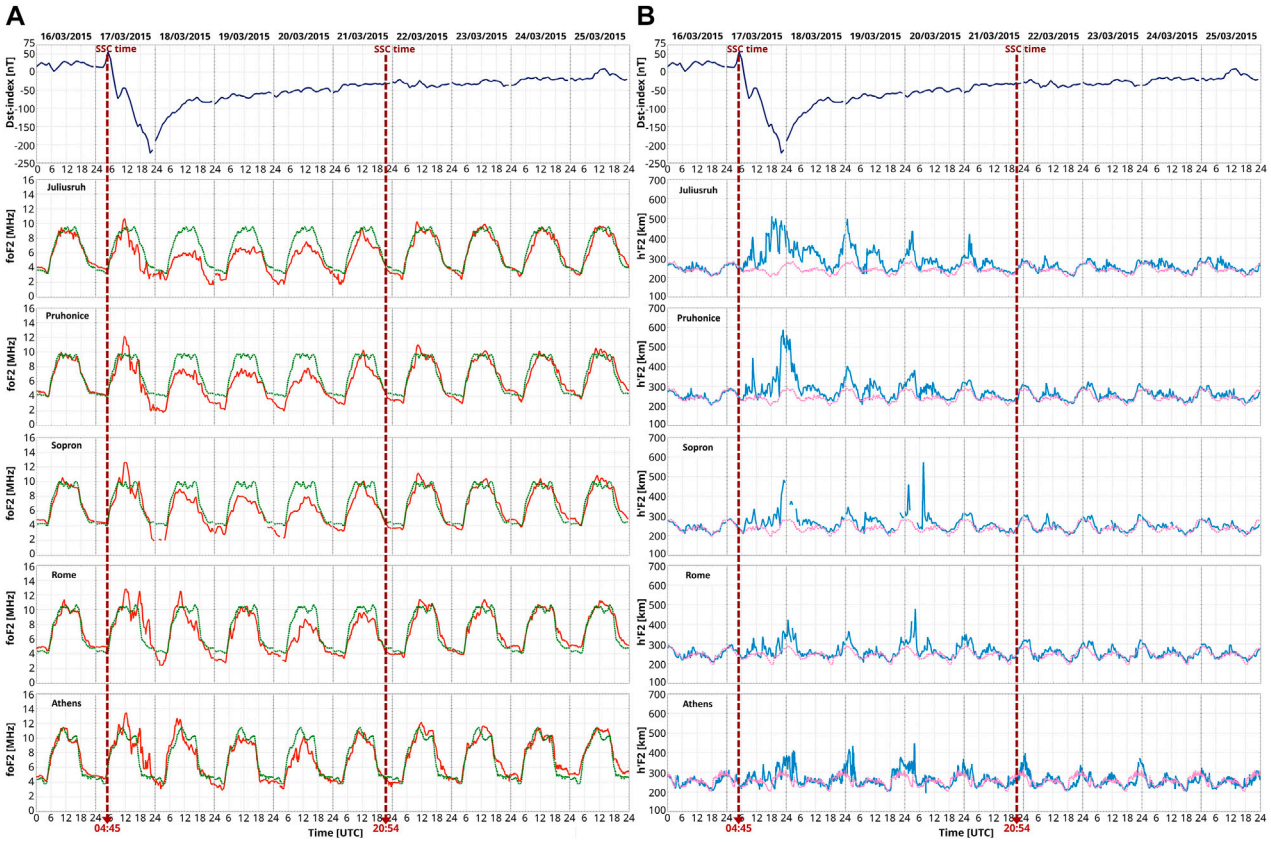

FIGURE 4
In the upper diagrams the Dst index values and in the other diagrams **(A)** the storm-time foF2 (red line) and **(B)** the storm-time h'F2 (light blue line) and the corresponding reference foF2 and h'F2 values (green **(A)** and pink **(B)**, respectively) are portrayed for the 2015 storm along the meridional chain.

days (during the early recovery phase) at SO, PQ and JR stations (middle - and high midlatitude), during both days and nights. Even at AT and RO, for a short period positive phase occurred around 9 UT, then it is turned into a significant negative phase around 11 UT. At RO and AT stations (low mid-latitude) the depletion became really significant (see Figure 4) only on 20 March. It can be stated that in the early recovery phase the low mid-latitude and the high mid-latitude regions behave differently.

A subsequent geomagnetic disturbance, associated with a HSSWS (see Figures 1, 4) started at 20:54 UT on 21 March, occurred during the recovery phase of the first storm and generated a positive ionospheric storm. Decreased electron density during the daytime and nighttime of 21th can be observed at all stations, but most significantly at RO. In the h'F2 parameter just a slight increase can be seen right after the SSC during the night, mostly at AT and RO stations. Meanwhile on 22 March no change was observed at JR, and only a slight increase in foF2 at PQ, SO, RO, AT. During the night the storm turns negative at all stations, except for RO and AT, where no change was observed.

During the remaining days in the recovery phase: on 23 March no changes at JR and PQ were detected, but a slight increase in foF2 at SO, RO, AT can be seen around noon. During the night just JR showed no changes, the others were positive. On 24 March no changes were observed in foF2 at all stations during the day, but at night just JR did not show changes, the other stations had positive phase. On 25 March the situation was the same as on day 23. The h'F2 parameter did not show any deviation from the QD curve during these days.

3.2 GNSS TEC data

To provide a wider context for the ionosonde observations, changes in the total electron content (TEC) data was compared with the foF2 values measured by the ionosondes. TEC data are presented similarly to Figures 3, 4 for a better comparison. The TEC represents the total electron content as an integrated value between the receiver on the ground and the GNSS satellite (MEO orbit, at around 20,000 km altitude), therefore it contains not just the whole ionosphere, but also most of the plasmasphere (Hofmann-Wellenhof and Lichtenegger, 2001).

In Figure 5 the TEC values (red) along with their corresponding references (green) for the 2012 November storm are plotted. Before the SSC time, on 11 and 12 November a small positive deviation can be seen during the day at all stations, while during the night on 11 November no significant deviation was observed. On the following night (12 November) a slight negative phase appeared at RO, SO and PQ. On 13 November, the day after the SSC, very impressive positive ionospheric storm phase developed at all stations during both day and night. In the main phase of the geomagnetic

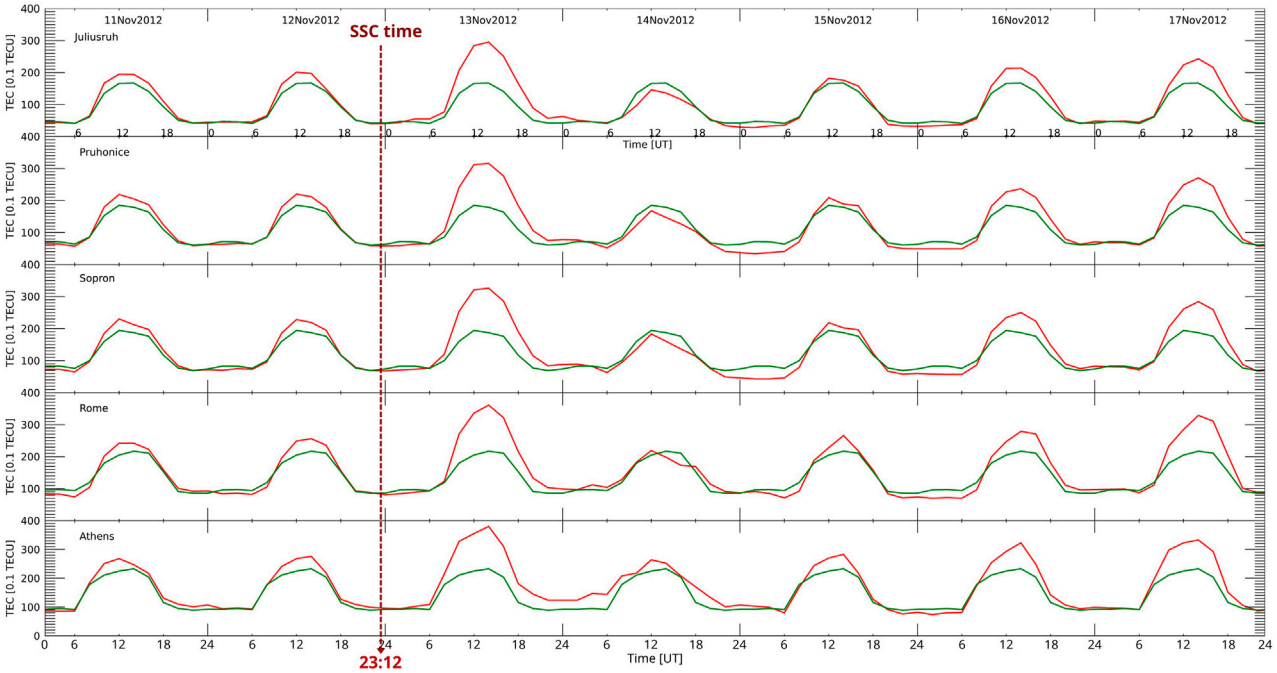

FIGURE 5
The meridional evolution of the storm-time GNSS TEC (with red line) with the reference TEC derived from selected 3 quiet days (with green line) are portrayed for storm 2012. SSC time is marked with a red dashed line.

storm (14 November) all stations turned negative except for RO, where there until 12 UT the TEC variation followed the mean variation. Later a slight decrease started and lasted until 18 UT. Also AT behaved differently, because here a TEC enhancement took place during the whole day. In the recovery phase (15–17 November) during the day positive phase was detected. On the contrary, during the nighttime hours on 15 November negative phase, and on 16 November no change was observed at all stations.

In Figure 6 the 2015 March storm can be seen in the TEC data. On the pre-storm day and night (16 March) no deviation from the reference values can be seen at any stations. In the main phase of the storm (17 March) significant positive phase is detected during the day at all stations, but during the night the storm phase is turned negative at all stations, except at JR where first a positive phase and then after midnight no deviation can be seen. During the early recovery phase between 18 and 20 March, a negative effect in TEC is detected during both day and night at all stations. Interestingly at RO and AT on 18 March between around 06–12 UT the TEC is increased with respect to the QD value, then rapidly decreases and stays decreased during the following 3 days. On 21 March the same effect was repeated during the day, but at night JR station showed no deviation, while all the other station data was negative. On 22 March (the day after the 2nd SSC) a positive ionospheric storm phase appeared in TEC during the day at all stations, but during the nighttime hours there was no effect. Between 23 and 25 March a slight positive phase can be seen during the day and night at all stations, except at JR where there is no effect during the night of 23 March.

The more specific connections are explained in the Discussion Section 4 below.

3.2.1 rTEC maps of the storms

In Figure 7 the Ratio of the TEC difference (rTEC) maps are shown for (geomagnetic) main phase of the two storms during the nighttime hours (18–04:00 UT). These maps show the relative deviation of TEC from its QD value (10 quietest days of the month). These rTEC maps clearly present the evolution of the nighttime negative phase along the examined stations in Europe.

In the case of the 2012 storm as shown in Figure 7A, the reduced electron density region moves from higher to lower latitudes, reaching its minimum latitude around midnight near the Athens-Rome line. Meanwhile, it is also nicely seen that the low-midlatitude Athens-Rome region remains in a positive phase throughout the night. In the 00:00 and 02:00 UT maps the depleted electron density zone is nicely drawn out in blue, and it can be seen that JR, PQ, SO stations are all located within it.

For the 2015 storm, a very strong positive phase (red color in Figure 7B) is visible at 18 UT on 17 March spreading in a NW-SE direction, its boundary shows up in yellow along the line connecting the Black See and North-France (see Figure 7B). SO, PQ to the North is green, indicating that there is no deviation from the expected value, while JR is in negative phase. Interestingly, there is a narrow but strong positive-phase region at high latitudes (over Scandinavia). As we move into the night, at 22:00 UT the negative phase moves towards the equator and the positive phase region also decreases in strength in the Athens-Rome line. At 00:00, the depleted plasma has gone even lower, and this is when both Rome and Athens go into negative phase at night, so the low mid-latitude region is also under the influence of this negative storm effect, which lasts until 04:00 UT.

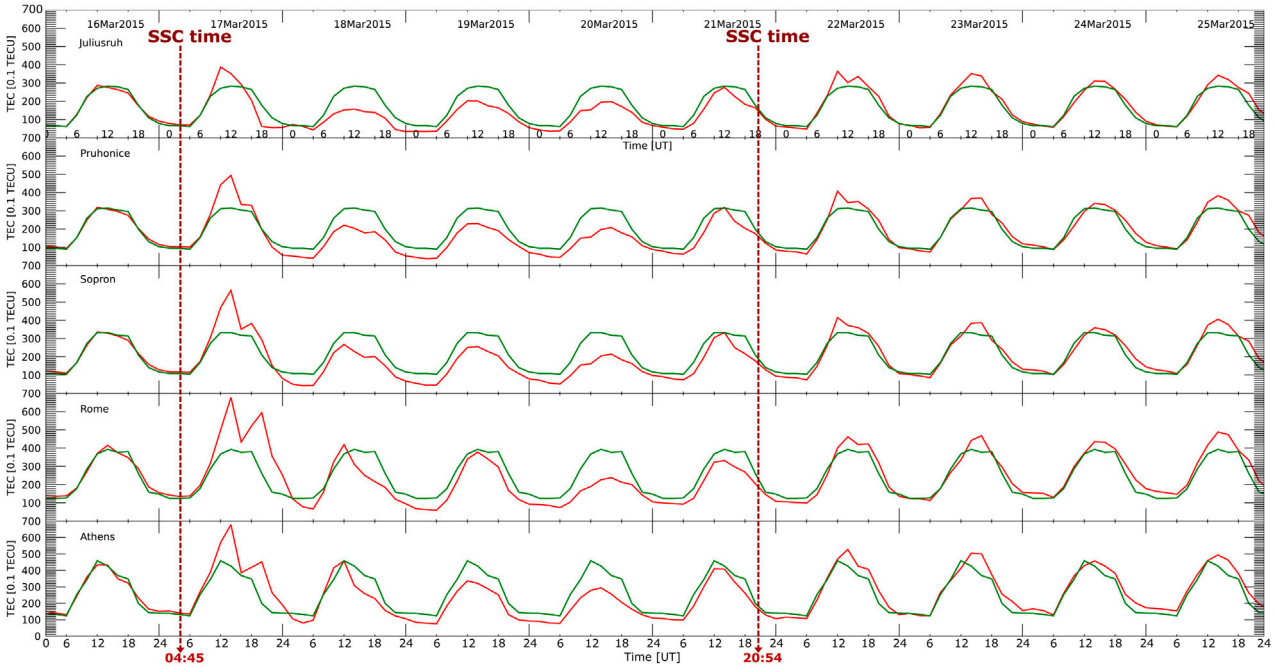

FIGURE 6
The meridional evolution of the storm-time GNSS TEC (with red line) with the reference TEC of selected 3 quiet days (with green line) are portrayed for storm 2015. SSC time is marked with red dashed line.

3.3 GUVI measurements

The TIMED satellite GUVI measurements were used to examine the variation of the daytime thermospheric O/N_2 composition during the evolution of the considered ionospheric storms. In Figures 8, 9 the three QDs as a reference are shown (Figure 8A; Figure 9A) and also 3 days from the storm (Figure 8B; Figure 9B) to present the main features. The whole storm intervals are plotted in Supplementary Figure S2 and Supplementary Figure S3 (note that time runs from right to left).

For the 2012 November storm the GUVI data presented in Figure 8 do not show any deviation in the O/N_2 ratio from the QD level over the examined stations during the daytime hours in the pre-storm phase (12 November). On 13 November (the day after the SSC) around noon (in LT) a slight increase in the O/N_2 (yellow) can be seen over Europe. In the main phase (when the Dst minimum value occurred), on 14 November around 12 LT, a significant decrease (blue) in the GUVI measured O/N_2 ratio can be observed all over Europe. On 15 November there is no deviation (green), but on 16 and 17 November a slight increase appears in GUVI data marked with yellow (see Supplementary Figure S2).

St. Patrick's Day storm 2015 (Figure 9): during the pre-storm phase was on 16 March, the O/N_2 ratio shows a decrease (blue) in the subauroral region, e.g., over JR station. After the SSC, during the main phase of the geomagnetic and ionospheric storm, on 17 March in the daytime GUVI data do not show any significant departure from the reference values.

On the contrary, during the following day, on 18 March, a quite deep depletion was observed in the O/N_2 ratio at JR, PQ and SO, but most significantly over the JR station. This effect also happens on the two following days just the same way, with one difference. On 20 March a slight depletion (light blue) showed up also at RO and AT stations (see Supplementary Figure S3). On 21 March, when the second SSC happened, another slight decrease follows in the GUVI data over JR, PQ, SO. During the next day, on 22 March, right over the JR station a slight decrease can be observed. On 23–25 March SO, PQ and JR stations are in the slightly depleted O/N_2 region (light blue) during the day.

3.4 Swarm satellite measurements

While ground ionosondes are good at monitoring the temporal variation of ionospheric parameters at fixed locations, LEO observations can provide pole-to-pole latitudinal profiles of the considered parameters recorded during around 45 min. The location of the plasmapause (PP), more precisely the location of ionospheric phenomena conjugated with PP, such as the MIT can also be monitored by LEO satellites (e.g., Heilig and Lühr, 2013; 2018; Heilig et al., 2022). Swarm observations are only available for the 2015 storm event. Figure 10 shows the change in the topside electron density (top panel) for three orbits of Swarm B, each separated by 9.5 h (in UT). All measurements were taken at around 21 h MLT but along different meridians. Thus this plot represents primarily the temporal evolution of the topside electron density at 21 h MLT, but the profiles are also influenced by longitudinal effects.

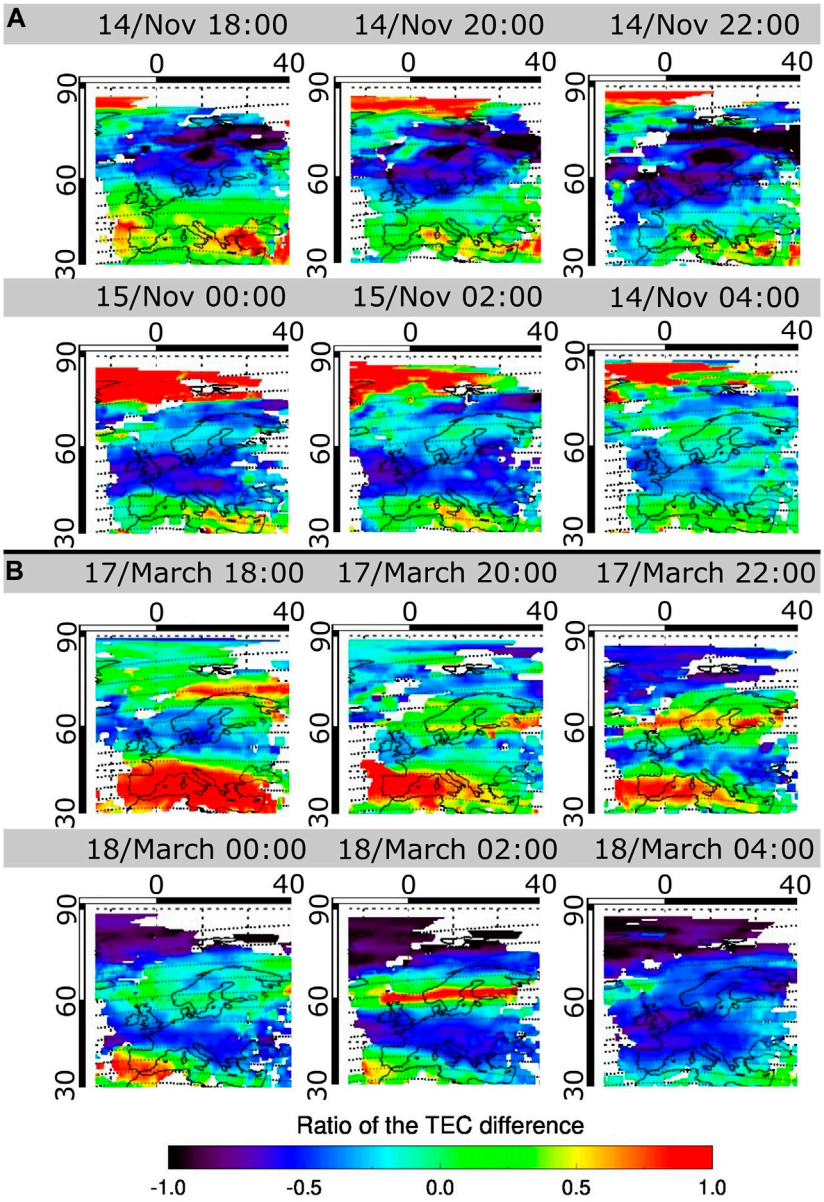

FIGURE 7
The rTEC values are plotted for the nighttime hours (18:00–04:00 UT) on 14 November, 2012 **(A)**, and on 17 March, 2015 **(B)**.

A deepening density minima (marked by vertical dashed lines on the Northern Hemisphere) can be observed in both hemispheres, moving progressively equatorward as the geomagnetic storm main phase develops. These are the minima of the MIT that is typically well observed in the nighttime ionosphere during equinoxes. Poleward of MIT, the erosion by the increased ExB drift continued along the whole day, while at lower latitudes at the altitude of Swarm B (505–525 km) a general increase was observed. The presented profiles were all taken following the SSC (04:45 UT). The latest profile corresponds to the time of the maximum of the plasmasphere erosion (most equatorward MIT).

Sharp MIT minima are accompanied by an enhanced electron temperature (bottom panel). This is a well-known feature of sub-auroral dynamics and appears mainly as a result of frictional heating by the intense westward drift that in turn are driven by an intense substorm (precipitation) associated poleward electric field (e.g., Heilig et al., 2022).

MIT minimum in this MLT sector is tightly coupled to the footprint of the plasmapause (Heilig et al., 2022). Thus the equatorward movement of MIT reflects the shrinking of the plasmasphere due to the increased magnetospheric convection and intensified substorm-related sub-auroral electric field (see also in Supplementary Figure S4).

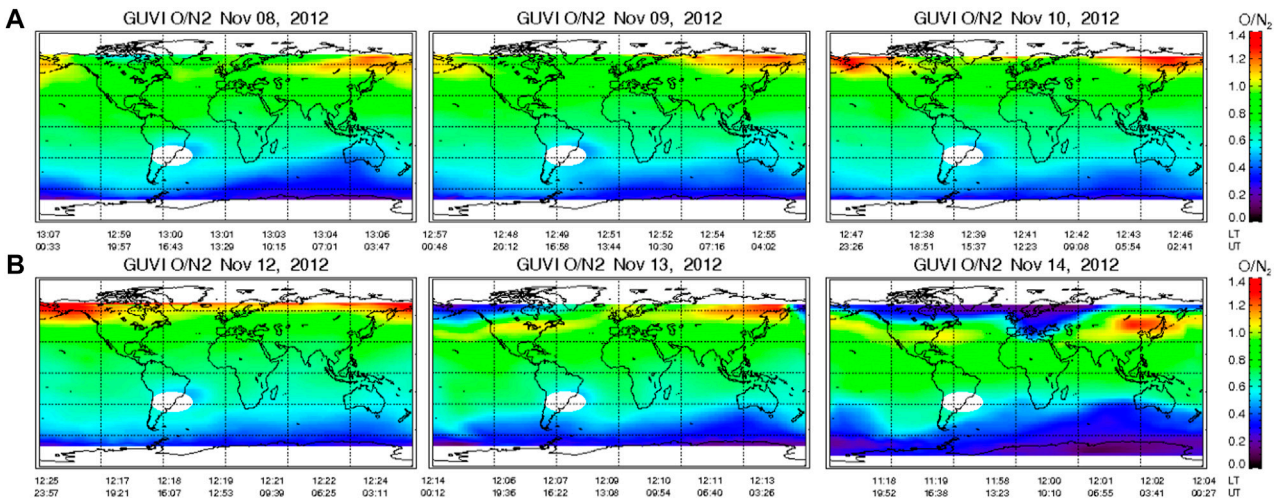

FIGURE 8
The GUVI measured O/N_2 ratio for the 2012 November storm. In the upper plot **(A)** reference data for 3 quiet days are shown; in the lower plots **(B)** data of 3 selected days from the storm interval are presented, namely, the day of SSC (12 November), the main phase of the ionospheric storm (13 November), and the main phase of the geomagnetic storm (14 November) (Note: a plot of GUVI data for the whole storm can be found in Supplementary Figure S1).

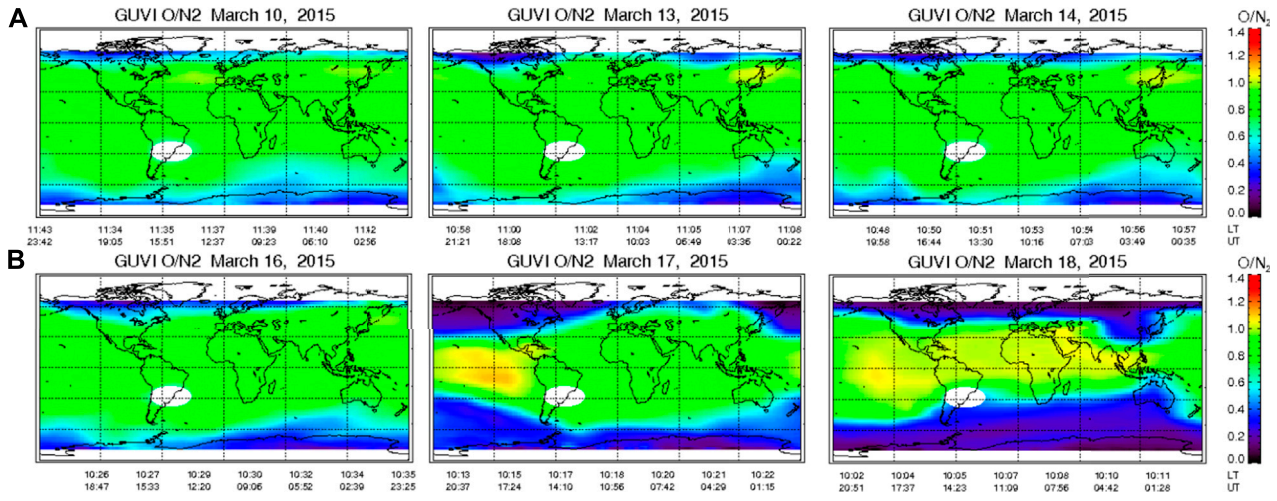

FIGURE 9
The GUVI measured O/N_2 ratio for the 2015 March storm. In the upper plot **(A)** reference data for 3 quiet days are shown; in the lower plots **(B)** data of 3 selected days from the storm interval are presented, namely, the day of pre-storm phase (16 March), the main phase of the ionospheric and geomagnetic storm (17 March), and 1 day from the recovery phase (18 March) (Note: a plot of GUVI data for the whole storm can be found in Supplementary Figure S2).

The time evolution of the MIT minimum position based on Swarm *in-situ* observations made on the Northern Hemisphere is presented in Figure 11. The two colors depict observations of Swarm B and C satellites. Right after the SSC, MIT started to shift equatorward. This decrease lasted the whole day, and by the end of the day MIT approached 45° magnetic latitude. The lowest latitude of the MIT position actually observed (by Swarm B) was 46.3°. This observation took place on 18 March at 00:15 UT (21.9 h MLT) at −43.2° longitude.

As shown in the lower panel, the MLT difference between Swarm B (red) and C (blue) observations was fairly stable, around 1.5 h on the average. The MIT position is well-known to have a strong MLT dependence (e.g., Heilig et al., 2022). The MIT latitude decreases during afternoon and also during nighttime until 4–6 h MLT. Here this dependence is reflected in the latitude difference between Swarm B and C observations, Swarm B observations are consequently equatorward of Swarm C observations by 2.3° on the average.

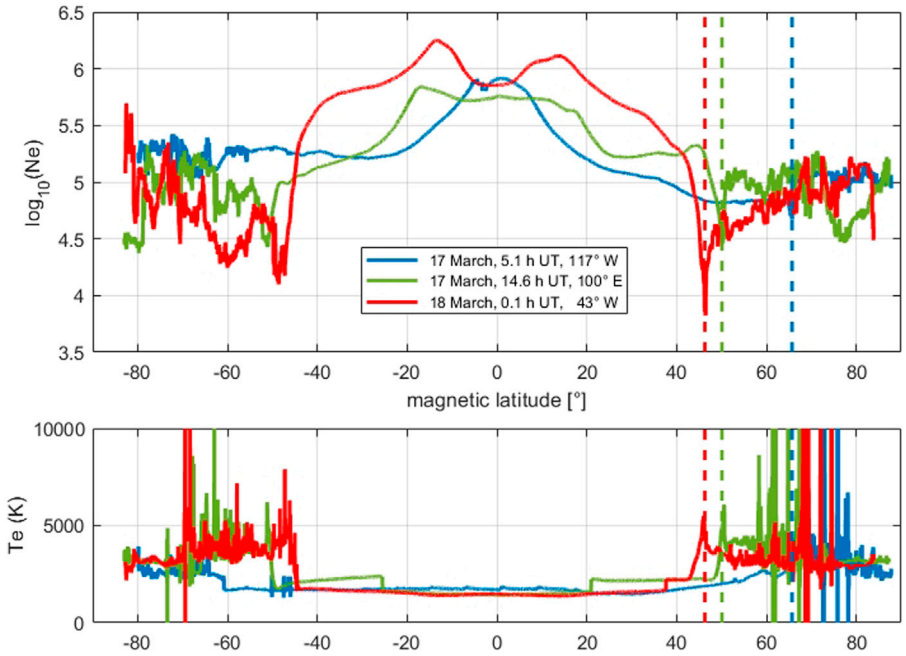

FIGURE 10
Meridional profiles of the topside electron density (top panel) and electron temperature (bottom panel) observed by Swarm B on 17 and 18 March, 2015. Vertical dashed lines indicate the location of MIT on the Northern hemisphere.

At the time of the minimum observation, MLT at Sopron was 0.72 h. Estimating from the MLT difference between Sopron and Swarm B (1.1 h) and the rate of decrease (2.3°/1.5 h = 1.53°/h), the MIT minimum at 0.72 h MLT was located around 45.6°. The formula (their Equation 4) of Deminov and Shubin (2018) for the MLT dependence yields a somewhat higher MIT latitude (45.9°). However, these values are already lower than the latitude of Pruhonice and very close to that of Sopron.

The MIT position is also known to depend on the geographic longitude (e.g., Heilig et al., 2022). In the American sector MIT appears a few degrees higher than in the European or Asian sector. The Equation 5 of Deminov and Shubin (2018) estimates this difference to 0.98°, while according to the statistical results of Karpachev et al. (2019), this difference could easily be 2°–3°. Using these adjustments the MIT at Sopron could have moved down as low as to magnetic latitude 44.6°, maybe even below 42°.

The width of the most equatorward MIT was 3.6° as observed by Swarm B. This width is shared between the equatorward wall (1.9°) and the poleward wall (1.7°). This means that on 17 March during the night MIT (but at least its equatorward wall) should have reached the Sopron station. Thus, the Sopron ionosonde observed the depleted plasma associated with the MIT structure. It is also clear that the MIT could not approach Athens, located at 36.1° magnetic latitude.

3.5 Digisonde drift measurements

Digisonde drift measurements from Pruhonice station were analyzed manually in order to determine the true horizontal and vertical motion of the F-layer during the two storm intervals. For the detailed analysis method of the manual correction see the Supplementary section. Now we are going to detail the phenomena found in the manual drift data for each storm separately.

The first significant manifestations of the 2012 November storm event can be seen on the drifts in the night from 13 to 14 November (Figure 12A). On 13 November around 20:30 UT a pronounced episode of westward drift begins. Roughly until 14 November 10:00 UT we observe dominantly horizontal westward drifts. The speed of the observed drifts is significantly higher than the horizontal speeds observed under quiet conditions (<100 m/s, according to Kouba and Koucka Knizova, 2012). The detected maximum speeds exceed even 350 m/s.

The quality of the skymap is very good and corresponds to the assumption of one drift velocity vector in the area above the station. Estimated vectors are determined reliably.

On 14 November around 00:00 UT, a significantly increased value of the vertical drift velocity component (to the tens of m/s) and its very rapid changes is added to the above-described effect. The drift measurement cadence was 15 min. The dramatic changes are visible in every consequent measurement, it is obvious that the period of the vertical drift velocity variation is significantly smaller than 15 min and cannot be studied (described) in more detail due to the limitations of the drift measurements.

During the day-time on 14 November both described manifestations practically disappeared. The value of the vertical velocity component no longer fluctuates quickly, and the value of the horizontal (westward) component drops to small values. Here it is necessary to note that the quality of measured skymaps during the

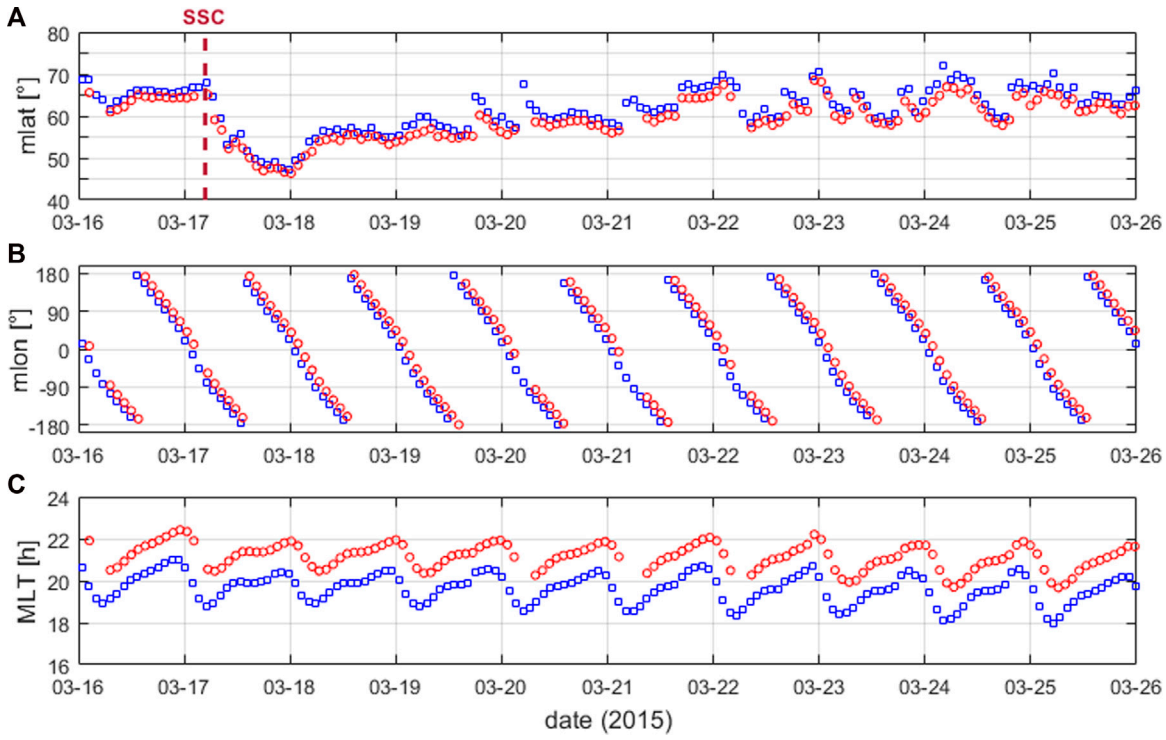

FIGURE 11
Evolution of the MIT minimum position (quasi dipole magnetic latitude) on the course of the 2015 event **(A)**; magnetic longitude **(B)** and MLT **(C)** of the *in-situ* Swarm observations. Red and blue colors depict Swarm B and C observations, respectively.

day-time is significantly lower than during the night-time. Therefore, information about the value of westward drift should be taken with a large margin. In most cases, the daytime skymap quality is not sufficient to determine the horizontal drift components with good reliability.

The second significant episode is observed during the night of 14/15 November This episode has similar characteristics, again between approx. 21:00 UT and 03:00 UT there is increased activity of the vertical component – larger values and rapid variations. In the horizontal components, a significant increase in the westward component can be seen again in the time interval between 23:00 – 08:00 UT. In this episode, the maximal measured values of the westward component exceed 250 m/s. It can be seen that the observed manifestations in the case of the second episode are smaller than in the case of the first.

In the drift measurements of 2015 March storm (Figure 12B), the first significant manifestations of the storm are observed on 17 March around 20:00 UT. The measurements show very quick variations of all observed parameters. The variations are significantly faster than the cadence of measurements and therefore the fluctuation period cannot be resolved. The value of the vertical drift velocity component exceeds the extreme values of +/- 50 m/s.

Unfortunately, in this phase of the storm, the actual extreme ionospheric situation (the values of foF2 and h'F2) does not allow successful realization of drift measurement in most cases. Between 22:00 UT and 01:00 UT successful measurements are rare.

During day-time 18 March no significant manifestations of the storm are observed in the drift measurements.

The next episode is coming at night 18/19 March. Rapid changes occur in the vertical component between 23:00 UT and 06:00 UT, and the amplitude of the vertical drift is significantly greater than values under normal conditions. In the horizontal component, we observe a pronounced westward peak between about 18:00 UT and 06:00 UT. The maximum detected values significantly exceed 200 m/s.

The last significant episode is observed the following night. On 20 March at around 00:00 – 04:00 UT the features described for the previous episode are repeated. It is interesting that this episode is significantly shorter than the previous one (roughly half) but the manifestations are more pronounced (on both the westward and the vertical components).

Drift activity affected by the storm is apparently observable also the following night (21 March, approx. 00:00 – 05:00 UT) on the westward component. The maximum detected velocity value is close to 200 m/s. In this case, however, the insufficient number of high-quality measurements does not allow proving a clear connection to the storm.

4 Discussion

In this section, we attempt to define the cause-effect relationships in order to gain a more detailed understanding of the response of the terrestrial ionosphere-plasmasphere system to geomagnetic storms. Our main focus was on the main phase of the geomagnetic storm, when during the night extremely depleted

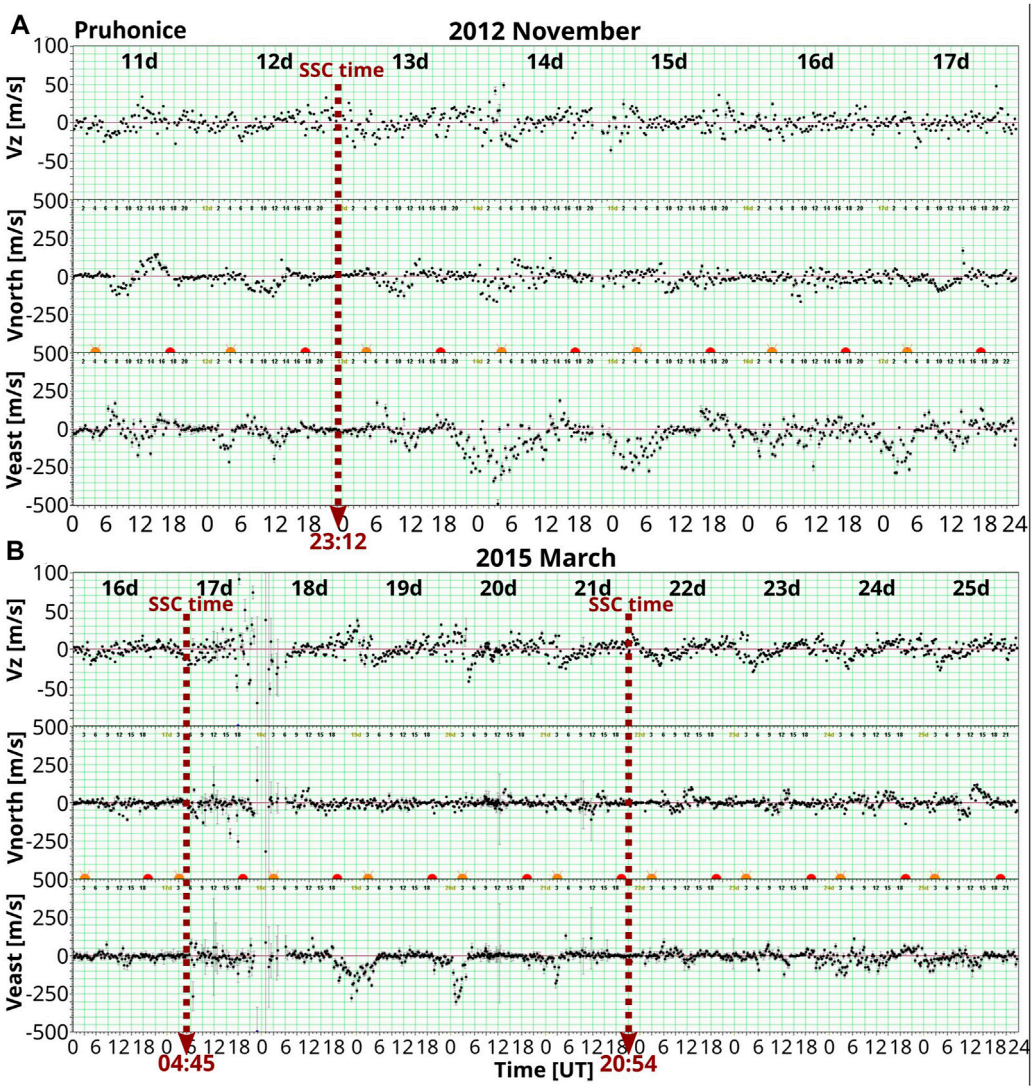

FIGURE 12
The manually corrected digisonde drift measurement of F-region for the 2012 November **(A)** and 2015 March **(B)** storm at Pruhonice station.

plasma was detected. Case studies are still important to shed light on deeper relationships that cannot be easily extracted from multi-event-based statistical investigations.

4.1 Pre-storm phase

In the pre-storm phase of the 2012 storm (11–12 November - Dst_{min} = 0 nT; Kp_{max} = 1,33; AE_{max} = 134 nT) foF2 and TEC show a slight positive deviation at all stations, while by the 2015 storm (16 March - Dst_{min} = 0 nT; Kp_{max} = 3,77; AE_{max} = 300 nT) no deviation from the reference value is detected. However, the O/N_2 data for this storm shows a decrease in the subauroral region already in this phase (16 March). Earlier studies (e.g., Kane, 1973a; Araujo-Pradere and Fuller-Rowell, 2002; Kane, 2005; Burešová and Laštovička, 2007) found a pre-storm feature (positive effect) in foF2 24 h before the SSC, however other authors doubt its presence (Mikhailov and Perrone, 2009). Burešová and Laštovička (2007) examined 65 strong geomagnetic storms from the period of 1995–2005 and found that about 20%–25% of the storms had a significantly strong pre-storm effect. Similarly to the finding of Liu et al. (2008), we found a slight pre-storm enhancement in both TEC and foF2 in the 2012 storm case. Other authors suggested that this effect could be related to some different channel of penetration of the energy from the interplanetary environment and magnetosphere to the ionosphere (Danilov and Belik, 1991; 1992; Blagoveshchensky and Kalishin, 2009), but this needs verification.

4.2 The main phase of ionospheric and geomagnetic storm

On the day right after the SSC (on 13 November 2012 - Dst_{min} = −29nT; Kp_{max} = 4,77; AE_{max} = 674 nT and on

17 March, 2015 - Dst_{min} = −234nT; Kp_{max} = 7,7; AE_{max} = 1570 nT) we observed a positive ionospheric storm phase at all station in both foF2 and TEC in both storms. This behavior is consistent with the average winter ionospheric response (in foF2 and TEC) to geomagnetic storms observed in previous studies (e.g., Matsuhita, 1959; Prölss, 1995; Buonsanto, 1999; Mendillo, 2006; Danilov, 2013). Astafyeva et al. (2015) examined the St. Patrick's Day storm's main phase (17–18 March) globally with multi-instrument measurements (e.g., Swarm VTEC, GUVI, GNSS TEC), and they found that the daytime positive phase during the day of 17 March at lower latitudes was due to increased O/N_2 ratio. This finding was also investigated and supported by Nayak et al. (2016); Kalita et al. (2016). The AE-index mostly exceeded 500 nT and increased often up to 1,500 nT during the day, which indicates the possibility of intense Joule heating of the thermosphere, which can cause positive storm phase by two ways: 1) the uplift of the layer through enhanced meridional winds, and then lift the ionization to greater heights (Prölss and Zahn, 1974). 2) the downwelling of atomic [O] causing the increase of O/N_2 ratio (see also in Introduction). Nava et al. (2016); Polekh et al. (2017) found also that the positive ionospheric effects at middle and low latitudes are related to different inputs of energy (as we see in AE-index; Figure 1B), and as they described the high latitude heating of the thermosphere travelled toward the equator with the velocity of 460 m/s during 17 March (along 120°E, see Polekh et al., 2017). Besides, Zhang S.R. et al. (2017a) found PPEF signatures on dayside over American sector, appearing as poleward/upward ion drift, and the observations showed meridional wind equatorward surges during also daytime hours. The upward ion drift could also contribute to the daytime positive phase (Zhang S.R. et al., 2017a). The diurnal evolution of the positive phase was different, dual peak can be seen at all stations. The first peak was at noon with maximum half hour delay, the second was around 18 h (UT). The second peak was observed (station-hour): JR-17 h, PQ and SO-17:30, RO and AT-18 h (UT). This could connected to the propagation of storm-induced electric field from north to south (e.g., PPEFs). After Kumar and Kumar (2022), eastward/westward PPEFs are associated with the southward/northward IMF Bz. The southward turnings of the IMF Bz component (induce eastward PPEF) can cause electron density increase during the daytime hours (Kumar and Kumar, 2022). There were two significant southward Bz episodes: around 8 and 14 (UT) during this time, which could support the above detailed assumption, but this needs verification.

For the 2012 November storm, the GUVI data show a slight increase in the O/N_2 over Europe on 13 November around LT noon (Figure 8), which could contribute to the positive phase in foF2 (Figure 3). There was a second peak (after the SSC) in AE-index with ~600 nT, which here indicates also the Joule-heating of the thermosphere. The generated processes here also could contribute to the positive phase similarly to 2015 storm by two ways. Unfortunately, there is no digisonde drift episode, which could strengthen the presence of uplifting of the layer or the enhanced equatorward meridional winds. This assumption needs verification also with Horizontal Wind Model 2007 (HWM07, Huang et al., 2018). Kumar and Kumar (2022) found that the PPEFs were contributors in the electron density increase during the day of 13 November, 2012. Interestingly, this day is the main phase of the ionospheric storm, and normally it develops on the course of the main phase of the geomagnetic storm, but by the 2012 storm, the geomagnetic storm's main phase was delayed by 1 day.

In the main phase of the geomagnetic storm in 2012 (14 November) during the daytime extremely depleted electron density was observed in foF2 at all stations. A similar decrease was observed also in TEC at all stations but with lower magnitude, except for AT and RO where it turned into negative only after 12 UT (see Figures 3, 5). Kane (2005) also found a deep decrease in electron density over the surrounding stations at midlatitude during the main phase of a similar storm (Dst_{min} = −589 nT). He also found that the magnitude of the Dst is not proportional to the magnitude of the negative effect in the ionosphere at middle and high-latitude. Pirog et al. (2006) strengthened it, where the analyzed geographic latitude range was similar to our case. The decrease of foF2 during the main phase of a geomagnetic storm is a known response of the ionosphere in winter, but usually during intense storms (Dst_{min}<= −100 nT) can reach lower latitudes (Danilov, 2013). According to the GUVI measurements around 12 LT a significant decrease of O/N_2 ratio was observed over Europe by GUVI (marked by blue in Figure 8). Generally, the main cause of a negative ionospheric storm is related to the depletion in the O/N_2 ratio, which is generated by the storm-time Joule-heating of the auroral thermospheric neutral gas leading to the formation of composition disturbance zone (with decreased O/N_2 rate) this zone is transported by the enhanced thermospheric meridional winds (TADs) equatorward (Seaton, 1956; Prölss and von Zahn, 1974; Mikhailov et al., 1989; Mikhailov et al., 1995; Prölss et al., 1995; Bunonsanto, 1999; Astafyeva et al., 2015). The third peak in AE-index with 1,000 nT happened at ~01:00 UT. This energy input could generate also Joule-heating of the thermosphere and this strengthen the possibility of our hypothesis. This is strengthening our earlier assumption that the main reason for the negative phase is due to the decreased O/N_2 ratio transported to lower latitudes (up to Sopron station) by meridional neutral winds (Berényi et al., 2018).

4.3 Deep electron density depletion during the night of 14 November and 17 March

Significantly eroded ionospheric plasma was detected during the nighttime hours in the main phase of the geomagnetic storms (from 18:00 UT on 14 November 2012 and from 20:43 on 17 March 2015) with short duration fade-out of the layers in the ionograms at some stations (detailed in section 3.1). The foF2 and TEC data show a clear negative phase at JR, PQ and SO stations in the 2012 November storm. On the contrary, a strong positive phase mainly in foF2 but slightly also in TEC at AT and RO stations was detected during the whole night of 14 November The rTEC maps of storm 2012 (Figure 7A) show the variation during the nighttime hours (18–4: 00 UT) on 14 November These rTEC maps show clearly how the reduced electron density region moves from the higher latitudes equatorward, reaching its minimum latitude around midnight along the Athens-Rome line. Between 00:00 and 02:00 UT, the depleted electron density region is very nicely drawn out, and it can be seen that JR, PQ and SO stations are fully located within it. In the meantime, the low-midlatitude Athens-Rome region remains in the positive phase throughout the night. Based on our observations and the findings of previous studies like Yizengaw et al. (2005), we can assume, that this nighttime positive phase at AT and RO region, is

caused by plasmasphere-ionosphere coupling due to the enhanced downward ExB drift (leading to a maintaining effect by the plasmasphere), which in the meantime led to a strong erosion of the plasmasphere. For the 2012 storm the drift measurements from PQ during that night shows the presence of a strong westward motion of F-layer plasma (v ~ 350 m/s) indicating the presence of the ionospheric trough (MIT) (see also Heilig et al., 2022). Thus we can conclude based on foF2 and drift data that the equatorward motion of the MIT region (so the PP footprint) was the main cause of the detected sharp electron density decrease in foF2, GNSS TEC and rTEC data during the night of the geomagnetic storm main phase at SO, PQ and JR stations. Another contributor was possibly also the depleted O/N_2 ratio, GUVI measurements show significant depletion above Europe during daytime, which could corotate with Earth (by westward winds) into the night sector, causing long-lasting negative phase (see Figure 8).

During the 2015 St. Patrick's Day storm both foF2 and TEC decreased at all stations during the night. In the rTEC maps, a very strong positive phase is visible at 18 UT on 17 March at lower latitudes, its boundary located along the line connecting the Black See and N-France (shown by yellow in Figure 7B). SO, PQ are in the green area, indicating that there is no deviation from the quiet level, as confirmed by the foF2 value (Figure 4). At the same time, JR is in negative phase, the foF2 shows significantly decreased electron density. It should be noted that the start time of the negative phase in TEC (and rTEC) was delayed by 3 h comparing it with the foF2 parameter at the same location. Based on the Swarm data (Figure 11) the MIT has already reached that latitude and it moved further to lower latitudes later, so it possibly caused the negative effect at JR. Previous studies indicated that the afternoon appearance of MIT may be linked to a plasmaspheric plume (see Heilig et al., 2022). According to the observed rTEC values, as we move into the night at 22:00 UT (note that in reality most possibly this happened ~01:00 UT based on the aforementioned 3 h delay in rTEC), the zone with depleted electron density moves towards the equator, and even the positive phase region has been pushed back in the Athens-Rome line. By 00:00, the depleted zone moved even lower, at this time both Rome and Athens go into negative phase based on the foF2 data, indicating that the low mid-latitude region is also under the influence of MIT. The location of the MIT reached the 44.6° magnetic latitude (or maybe even below 42°) at 0.72 h MLT based on Swarm electron density and temperature measurements (Figures 10, 11) and the method described in Heilig et al. (2022). This sharp MIT minima was also accompanied by increased electron temperature with more than 5000 K (Figure 10), which was also observed by Liu et al. (2016), Zhang S.R. et al. (2015, Zhang S.R. et al. (2017a) during 16–19:30 UT on 17 March, which was presumably caused by strong frictional heating due to large plasma drifts. The equatorward motion of the minima of MIT is indicating that the plasmasphere was shrinking (see also Supplementary Figure S4), and the stations (JR, PQ, SO) went outside the plasmasphere where the ionosphere was not filled any more from the plasmasphere leading to extremely decreased electron density (detailed in Section 2). The severely depleted ionosphere was conjugated to the depleted outer magnetosphere (plasma trough) (see also Heilig et al., 2022). The F-layer drift measurement (at PQ) detected an intense ~500 m/s speed westward drift from appr. 20–02:00 UT (see Figure 12B) which is associated with the MIT formation mechanism. The effect of MIT lasts until 04:00 UT. Our findings are in good agreement with the results of previous articles like Nayak et al. (2016), who examined the equatorward motion of the MIT in the American sector (reached up to 40° N latitude) and Huang et al. (2018) also observed obvious westward disturbances in the zonal wind over central China (Asia, 38.7°N, 111.6°E). From 22:00 -02:00 UT strong westward neutral wind appeared, and at 03:00 UT a poleward wind surge of ~100 m/s appeared due to the poleward Coriolis force arising from the significant westward wind amplitudes (see Zhang S.R. et al., 2015; Tulasi et al., 2016; Huang et al., 2018). These were found to be driven by strong SAPS westward ion drift of >500 m/s peaking in the MIT and were accompanied by > 50 m/s upward ion drift in the E– and F-layers during SAPS periods at 22:43 UT at subauroral and midlatitudes (Zhang S.R. et al., 2015; Zhang S.R. et al., 2017a). But at lower latitudes poleward winds might not be driven by SAPS, most probably these wind changes are associated with travelling atmospheric disturbances (TADs) originated from the disturbance source region in the southern hemisphere (Huang et al., 2018).

After the observation of Zhang S.R. et al. (2017a) the SED plume over America (Millstone Hill) 20–24 UT can be linked to the positive phase over Southern Europe (AT and RO) from 18–22 UT: the westward winds could bring the plasma from Europe to North America leading to the detected SED plume over there (see Figure 4; Figure 7B) within a few hours, however, PPEF may also play some role in its formation (Liu et al., 2016). Investigation of Liu et al. (2016) and model results of Lu et al. (2020) confirm this possibility. Interestingly, a strong positive-phase region appeared at high latitudes (over Scandinavia), which can represent the poleward boundary of the MIT. The data show positive deviation, partly because the electron density was quite low in that region during QDs, while during the subsequent storm a quite significant increase took place in association with the equatorward movement of the MIT.

To speak about the lower latitudes, previous studies found the cumulative effect of enhanced meridional wind and changes in the electric fields, during night of the main phase at the 30–40°N zone. At low latitudes (like RO and AT) the detected variations in the ionosphere were governed by the superposition of disturbed electric fields (DDEFs), and the PPEF, which triggered the drop of foF2 in the evening on 17 March and the morning on 18 March (see Astafyeva et al., 2016; Jin et al., 2017; Polekh et al., 2017). For the St. Patrick's Day storm, the ionospheric effects of PPEF to low latitudes and the ionospheric disturbance dynamo (DDEF) were examined and discussed by several other papers: Le Huy and Amory-Mazauider, (2008); Lu et al. (2012); Abdu et al. (2013); Nava et al. (2016); Nayak et al. (2016); Ramsingh et al. (2015); Ram et al. (2016); Kalita et al. (2016). This could contribute to the nighttime electron density decrease at lower latitudes (AT, RO).

4.4 Recovery phase

During the recovery phase (on 15–17 November 2012 - Dst_{min} = −40;-27;-13nT; Kp_{max} = 1,33; 2,77; 3; AE_{max} = 119; 310; 328 nT and 18–20 March 2015 - Dst_{min} = −200;-99;-81 nT; Kp_{max} = 6; 5;4,77; AE_{max} = 1,043; 1,134; 611 nT) all station's TEC and foF2 data showed a positive phase in the 2012 storm case, while

they showed a significant negative phase in the 2015 St. Patrick storm case. Yizengaw et al. (2005) examined a geomagnetic storm from 31 March, 2001 (Dst_{min} = −380 nT) and found also an extended, long-lasting negative phase during the recovery phase. The reason for the long-lasting negative phase during storm 2015 can be the great extension of composition disturbance zone to low latitudes as suggested by Danilov (2013 and references therein). These statements are also confirmed by our analysis of GUVI data. On 18 March, 2015, a quite deep depletion was observed in O/N_2 ratio over Juliusruh (Figure 9) accompanied by foF2 decrease (Figure 4). The effect also re-occurs on 19 March, moreover the foF2 parameter data show a slight depletion also at PQ, SO and RO on 20 March. Nava et al. (2016), Huang et al. (2018) and Chernigovskaya et al. (2021) also found this depletion in electron density (18–20 March). They found that, during the recovery phase the important role in dynamics of the midlatitude ionosphere may belong to the wave-like thermospheric disturbances of molecular gas, propagating westward for several days causing electron density decrease along the trajectories of propagation. Besides, after the investigation of Kumar and Kumar (2019) another contributor to formation of the negative phase can be related to DDEFs. As for the 2012 storm, a negative phase changed to a positive one, which is believed to be caused by travelling atmospheric disturbances (TADs) (Danilov, 2013). These are generally brought by the same storm-time equatorward meridional wind discussed above, and have velocity of about 440 m/s (Mansilla, 2003). These processes uplift the layer to greater altitude, where the loss rate is lower, beside there is downwelling in atomic [O], resulting in an increase in electron density. On 16–17 November a slightly increased O/N_2 was observed by GUVI (marked with yellow in Figure 8), which could contribute to the daytime positive effect in foF2 around 10–15 UT at all investigated stations (Figure 3; see also article of Illes-Almar et al., 1987; Pirog et al., 2006).

The 2015 storm was followed by a second SSC by an HSSWS happened on 21 March at night. During that day, a negative phase was detected at all stations in both TEC and foF2 but not any disturbance was observed in GUVI data. One day later (Dst_{min} = −56 nT; Kp_{max} = 6.33; AE_{max} = 1078 nT) a slight positive phase was present both in TEC and in foF2 at all stations. During the remaining days in the recovery phase, foF2 data do not show significant departure from the QD values, while in TEC a slightly positive effect was recorded. The possible reason for the late recovery phase behavior may be linked to the fact that the examined European stations were then inside the plasmasphere during the daytime. Thus the effect of the composition change could have been suppressed by other factors. Another possible reason could be that the HSSWS caused electron density increase during the first 2 days. Nava et al. (2016) found that the HSSWS event is added some energy into the magnetosphere, extending the lifetime of the recovery phase.

We detail the observed diversities between foF2 and TEC during the daytime and nighttime of the two storms in the Supplementary section. The differences between the behavior of the foF2 parameter and TEC can be linked to the fact that TEC includes the plasma not only from the topside ionosphere (from above the height of foF2 parameter - hmF2) but also from plasmasphere. It is generally accepted that about 2/3 of the integrated TEC comes from the region above hmF2 (Mendillo, 2006). Due to this fact TEC is the best for portraying, assessing and understanding the overall behavior of the near-Earth thermal plasma (ionosphere and plasmasphere) (Mendillo, 2006). It has to be mentioned here that TEC plots used for this study (on Figures 5, 6) are based on a TEC grid map (not from individual GNSS stations). The plotted values are taken at a grid point (closest to each ionosonde station) of these TEC maps, so it is a smoothed interpolated value that can also be a reason for that it is less sensitive than the foF2 measured at individual stations.

In future studies, we found important to compare these results with some existing models/simulations in order to analyze and test the aforementioned processes: with NRL ionosphere/plasmasphere model SAMI3 (Huba et al., 2017), the thermosphere-ionosphere-electrodynamic general circulation model (TIEGCM, see the article of Lu et al., 2020), Horizontal Wind Model 2007 (HWM07, Huang et al., 2018), Global Self-consistent Model of the Thermosphere, Ionosphere, and Protonosphere (GSM TIP, Ratovsky et al., 2019) and also with the simulations of Fuller-Rowell et al. (1994) and Forbes and Roble et al. (1990). It is important mainly for the 2012 storm case where we do not have Swarm satellite measurement, and Fabry–Perot interferometer neutral wind observations to confirm our assumptions about the possible ionospheric effect drivers.

5 Conclusion

During the evolution of two ICME-related geomagnetic storms, we investigated the extent of disturbances in the ionosphere. Our supreme aim was to find connections between geomagnetic storm induced processes in the ionosphere and to determine the evolution of the effects over Europe through a meridional chain of digisondes. We used various measurements (GNSS TEC, GUVI, Swarm, digisonde drift data) to find the possible cause of the detected features. The results of this study are summarized below:

[1] On 13 November 2012: the thermospheric composition changes and PPEFs contributed to the evolution of the daytime positive phase at all stations. Drift measurements from Pruhonice indicate the presence of the ionospheric trough (MIT) between 20:30–10:00 UT, reflected in the westward motion of the F-layer plasma with a velocity of 350 m/s, which was the main cause of the depletion in foF2 during the postmidnight sector at JR, PQ and SO.

[2] On 17 March 2015, a daytime positive ionospheric storm developed at all stations except at JR. We can conclude that the negative phase at JR is a consequence of the equatorward motion of the MIT during the daytime. By GUVI data we assume that the composition change possibly had no effect. We assume that the possible cause of the positive phase was mainly connected to the Joule-heating of the auroral thermosphere, which lifted up the plasma through enhanced equatorward winds to altitudes where chemical loss rate of ions are slow. Besides, after previous studies, one of the cause was most possibly the PPEFs. The observed virtual height variation and the vertical drift data along with previous studies also confirms the uplifting scenario.

[3] On 14 November 2012: in foF2 data the negative phase is extremely significant at all stations from 6 UT till the afternoon hours. Based on the GUVI data, this effect is related to a very strong decrease in O/N_2 ratio during the day.
[4] During the night of the 14 November, 2012 we found that the presence of the midlatitude ionospheric trough (MIT) was the primary reason for the formation of the negative phase at JR, PQ, SO stations. The rTEC maps and the drift measurements at PQ also confirms the presence of a nighttime trough. In addition, based on the GUVI data the daytime compositional disturbance zone seems to extend equatorward during the night, contributing to a more pronounced electron density drop.
[5] The location of MIT minima (coincides with the ionospheric footprint of the PP) is likely reached the latitude of Sopron at night of 14 November according to the data. On the contrary AT and RO remained inside the plasmasphere, appearing as increase in foF2. It is in line with previous studies.
[6] Swarm data together with the digisonde drift measurements support our hypothesis that the extreme decrease in foF2 and TEC at night of 17 March is related to the equatorward motion of the MIT along with the intense SAPS westward ion drift, as MIT went down to 44.6° (or even below 42°) geomagnetic latitude at 0.72 h MLT. This condition resulted in an even pronounced electron density drop in the ionosphere above SO and PQ. The decreased O/N_2 ratio also contributed to the depletion effect.
[7] After the observation of previous studies, the SED plume over America (at subauroral latitudes) between 20 and 24 UT on 17 March can be linked to the positive phase (SED) from 18–22 UT in foF2 and rTEC over Southern Europe (RO and AT): the westward winds could bring the plasma from Europe to North America leading to the detected SED plume over there.
[8] By the 2012 storm" recovery phase, the variation from the daytime positive to negative phase in foF2 and TEC is probably due to the change in the neutral composition.
[9] The foF2 and TEC data are similar in their main patterns during the two investigated geomagnetic storms.
[10] The combined analysis of Swarm, rTEC, drift and foF2 measurements give another method beside the existing ones of previous researchers to monitor the evolution and movement of the ionospheric features like MIT (the ionospheric footprint of the plasmapause), SED and SAPS. This can deepen our understanding of the processes during different geomagnetic storms, and could be use in the future in space weather prediction models.
[11] In future studies, we found important to compare these results with some existing models/simulations in order to analyze and test the aforementioned processes.

Data availability statement

The datasets presented in this study can be found in online repositories. The names of the repository/repositories and accession number(s) can be found below (accessed on 09 March 2023): The IMF Bz and SW data and also Dst-, Kp-, and AE-index are from OMNIWEB (http://omniweb.gsfc.nasa.gov/form/dx1.html) with a resolution of 1 h and 1 min, as well as from WDC Kyoto (https://wdc.kugi.kyoto-u.ac.jp/dst_final/index.html). International Q-days (QD) list (https://wdc.kugi.kyoto-u.ac.jp/qddays/), geomagnetic coordinate calculator (https://wdc.kugi.kyoto-u.ac.jp/igrf/gggm/index.html), GIRO scaled digisonde parameters (https://giro.uml.edu/didbase/scaled.php) and for drift data (https://giro.uml.edu/driftbase/), GUVI data available at http://guvitimed.jhuapl.edu/data_fetch_l3_on2_gif, Swarm satellite constellation, Langmuir Probe data are available at: (https://earth.esa.int/eogateway/missions/swarm/product-data-handbook/preliminary-level-1b-plasma-dataset).

Author contributions

KB was the main organizer and writer of this article, and responsible for the manual correction of all ionosonde data used for the analysis. VB contributed to the structure of the research, the basic concept, checked the workflow and improved the manuscript. BH performed the analysis of Swarm satellite data, added figures. JU selected and plotted the GNSS TEC data. DK manually corrected the digisonde drift measurements and wrote the description for it. ÁK supported the first author with ideas and fundings. All members contributed substantially to science discussion and manuscript development.

Funding

This article is supported by the NKM55/2018 MTA mobility tender. Global GNSS-TEC data processing has been supported by JSPS KAKENHI Grant Number 16H06286. The contribution of VB was supported by OTKA, Hungarian Scientific Research Fund (grant no. PD 141967) of the National Research, Development and Innovation Office and by Bolyai Fellowship (GD, no. BO/00461/21). Furthermore, her work was supported by the GINOP-2.3.2-15-2016-00003 project.

Acknowledgments

We thank the data centers (OMNIWEB and WDC for Geomagnetism, Kyoto) and the Széchenyi István Geophysical Observatory at Nagycenk, Hungary, Athens (AT138), Rome (RO041), Pruhonice (PQ052) and Juliusruh (JR055) station for supplying high quality ionosonde and digisonde data for the research. The GUVI instrument was designed and built by The Aerospace Corporation and The Johns Hopkins University. The Principal Investigator is Dr. Andrew B. Christensen and the Chief Scientist and co-PI is Dr. Larry J. Paxton. GNSS RINEX files for the GNSS-TEC processing are provided from many organizations listed by the webpage (http://stdb2.isee.nagoya-u.ac.jp/GPS/GPS-TEC/gnss_provider_list.html). Also we are grateful for the reviewers for their valuable advices, which improved our article. The GUVI data used here are provided through support from the NASA MO&DA program.

Conflict of interest

The authors declare that the research was conducted in the absence of any commercial or financial relationships that could be construed as a potential conflict of interest.

Publisher's note

All claims expressed in this article are solely those of the authors and do not necessarily represent those of their affiliated organizations, or those of the publisher, the editors and the reviewers. Any product that may be evaluated in this article, or claim that may be made by its manufacturer, is not guaranteed or endorsed by the publisher.

Supplementary material

The Supplementary Material for this article can be found online at: https://www.frontiersin.org/articles/10.3389/fspas.2023.1092850/full#supplementary-material

References

Aa, E., Zou, S., Erickson, P. J., Zhang, S.-R., and Liu, S. (2020). Statistical analysis of the main ionospheric trough using Swarm *in situ* measurements. *J. Geophys. Res. Space Phys.* 125, e2019JA027583. doi:10.1029/2019JA027583

Abdu, M. A., Souza, J. R., Batista, I. S., Fejer, B. G., and Sobral, J. H. A. (2013). Sporadic E layer development and disruption at low latitudes by prompt penetration electric fields during magnetic storms. *J. Geophys. Res. Space Phys.* 118, 2639–2647. doi:10.1002/jgra.50271

Araujo-Pradere, E. A., and Fuller-Rowell, T. J. (2002). Storm: An empirical storm-time ionospheric correction model, 2. Validation. *Radio Sci.* 37 (5), 4-1–4-14. doi:10.1029/2002RS002620

Astafyeva, E., Zakharenkova, I., and Alken, P. (2016). Prompt penetration electric fields and the extreme topside ionospheric response to the June 22–23, 2015 geomagnetic storm as seen by the Swarm constellation. *Earth Planet Sp.* 68, 152. doi:10.1186/s40623-016-0526-x

Astafyeva, E., Zakharenkova, I., and Förster, M. (2015). Ionospheric response to the 2015 St. Patrick's day storm: A global multi-instrumental overview. *J. Geophys. Res. Space Phys.* 120, 9023–9037. doi:10.1002/2015JA021629

Berényi, K. A., Barta, V., and Kis, V. (2018). Midlatitude ionospheric F2-layer response to eruptive solar events-caused geomagnetic disturbances over Hungary during the maximum of the solar cycle 24: A case study. *Adv. Space Res.* 61, 1230–1243. doi:10.1016/j.asr.2017.12.021

Blagoveshchensky, D. V., and Kalishin, A. S. (2009). Increase in the critical frequency of the ionospheric F region prior to the substorm expansion phase. *Geomagn. Aeron.* 49, 200–209. doi:10.1134/S0016793209020091

Bór, J., Sátori, G., Barta, V., Szabóné-André, K., Szendroi, J., Wesztergom, V., et al. (2020). Measurements of atmospheric electricity in the Széchenyi István geophysical observatory, Hungary. *Hist. Geo-and Space Sci.* 11 (1), 53–70. doi:10.5194/hgss-11-53-2020

Buonsanto, M. J. (1999). Ionospheric storms – a review. *Space Sci. Rev.* 88, 563–601. doi:10.1023/a:1005107532631

Burešová, D., and Laštovička, J. (2007). Pre-storm enhancements of foF2 above Europe. *Adv. Space Res.* 39, 1298–1303. doi:10.1016/j.asr.2007.03.003

Cherniak, I., and Zakharenkova, I. (2015). Dependence of the high-latitude plasma irregularities on the auroral activity indices: A case study of 17 March 2015 geomagnetic storm. *Earth Planet Sp.* 67, 151. doi:10.1186/s40623-015-0316-x

Chernigovskaya, M. A., Shpynev, B. G., Yasyukevich, A. S., Khabituev, D. S., Ratovsky, K. G., Belinskaya, A. Yu., et al. (2021). Longitudinal variations of geomagnetic and ionospheric parameters in the Northern Hemisphere during magnetic storms according to multi-instrument observations. *Adv. Space Res.* 67, 762–776. doi:10.1016/j.asr.2020.10.028

Christensen, A. B., Paxton, L. J., Avery, S., Craven, J., Crowley, G., Humm, D. C., et al. (2003). Initial observations with the global ultraviolet imager (GUVI) in the NASA TIMED satellite mission. *J. Geophys. Res.* 108, 1451. doi:10.1029/2003JA009918,A12

Crowley, G., Hackert, C. L., Meier, R. R., Strickland, D. J., Paxton, L. J., Pi, X., et al. (2006). Global thermosphere-ionosphere response to onset of 20 November 2003 magnetic storm. *J. Geophys. Res.* 111, A10S18. doi:10.1029/2005JA011518

Danilov, A. D., and Belik, L. D., (1991). Thermosphere-ionosphere inter-action in a period of ionospheric storms, *Geomagn. andAeronomy*, 31, 157–167.

Danilov, A. D., and Belik, L. D. (1992). Thermospheric composition and the positive phase of an ionospheric storm. *Adv. Space Res.* 12 (10), 257–260. ISSN 0273-1177. doi:10.1016/0273-1177(92)90475-D

Danilov, A. D. (2013). Ionospheric F-region response to geomagnetic disturbances. *Adv. Space Res.* 52, 343–366. doi:10.1016/j.asr.2013.04.019

Deminov, M. G., and Shubin, V. N. (2018). Empirical model of the location of the main ionospheric trough. *Geomagn. Aeron.* 58, 348–355. doi:10.1134/S0016793218030064

Forbes, J. M., and Roble, R. G. (1990). Thermosphere-ionosphere coupling: An experiment in interactive modeling. *J. Geophys. Res.* 95 (A1), 201. doi:10.1029/JA095iA01p00201

Fuller-Rowell, T. J., Codrescu, M. V., Moffett, R. J., and Quegan, S. (1994). Response of the thermosphere and ionosphere to geomagnetic storms. *J. Geophys. Res.* 99 (A3), 3893–3914. doi:10.1029/93JA02015

Habarulema, J. B., Yizengaw, E., Katamzi-Joseph, Z. T., Moldwin, M. B., and Buchert, S. (2018). Storm time global observations of large-scale TIDs from ground-based and *in situ* satellite measurements. *J. Geophys. Res. Space Phys.* 123, 711–724. doi:10.1002/2017JA024510

Hairston, M., Coley, W. R., and Stoneback, R. (2016). Responses in the polar and equatorial ionosphere to the March 2015 St. Patrick Day storm. *J. Geophys. Res. Space Phys.* 121, 11,213–11,234. doi:10.1002/2016JA023165

He, M., Liu, L., Wan, W., and Zhao, B. (2011). A study on the nighttime midlatitude ionospheric trough. *J. Geophys. Res. Space Phys.* 116, 5315. doi:10.1029/2010ja016252

Heilig, B., and Lühr, H. (2013). New plasmapause model derived from CHAMP field-aligned current signatures. *Ann. Geophys.* 31, 529–539. doi:10.5194/angeo-31-529-2013

Heilig, B., and Lühr, H. (2018). Quantifying the relationship between the plasmapause and the inner boundary of small-scale field-aligned currents, as deduced from Swarm observations. *Ann. Geophys.* 36, 595–607. doi:10.5194/angeo-36-595-2018

Heilig, B., Stolle, C., Kervalishvili, G., Rauberg, J., Miyoshi, Y., Tsuchiya, F., et al. (2022). Relation of the plasmapause to the midlatitude ionospheric trough, the sub-auroral temperature enhancement and the distribution of small-scale field aligned currents as observed in the magnetosphere by THEMIS, RBSP, and arase, and in the topside ionosphere by Swarm. *J. Geophys. Res. Space Phys.* 127, e2021JA029646. doi:10.1029/2021ja029646

Hofmann-Wellenhof, B., and Lichtenegger, H. (2001). "Global positioning system," in *Theory and practice* (Australia: Flinders University).

Horváth, I., and Lovell, B. C. (2016). Structured subauroral polarization streams and related auroral undulations occurring on the storm day of 21 January 2005. *J. Geophys. Res. Space Phys.* 121, 1680–1695. doi:10.1002/2015JA022057

Huang, C., Xu, J-Y., Zhang, X-X., Liu, D., Yuan, W., and Jiang, G-Y. (2018). Mid-latitude thermospheric wind changes during the St. Patrick's Day storm of 2015 observed by two Fabry-Perot interferometers in China. *Adv. Space Res.* 61 (7), 1873–1879. doi:10.1016/j.asr.2017.10.013

Huba, J. D., Sazykin, S., and Coster, A. (2017). Sami3-RCM simulation of the 17 March 2015 geomagnetic storm. *J. Geophys. Res. Space Phys.* 122, 1246–1257. doi:10.1002/2016JA023341

Illes-Almar, E., Almar, I., Bencze, P., and Horváth, A. (1987). Investigation of the thermosphere-ionosphere interaction by means of the neutral post-storm effect. *Adv. Space Res.* 7, 53–57. doi:10.1016/0273-1177(87)90189-x

Immel, T. J., and Mannucci, A. J. (2013). Ionospheric redistribution during geomagnetic storms. *J. Geophys. Res. Space Physics* 118, 7928–7939. doi:10.1002/2013JA018919

Jin, S., Jin, R., and Kutoglu, H. (2017). Positive and negative ionospheric responses to the March 2015 geomagnetic storm from BDS observations. *J. Geod.* 91, 613–626. doi:10.1007/s00190-016-0988-4

Kalita, B. R., Hazarika, R., Kakoti, G., Bhuyan, P. K., Chakrabarty, D., Seemala, G. K., et al. (2016). Conjugate hemisphere ionospheric response to the St. Patrick's Day storms of 2013 and 2015in the 100°E longitude sector. *J. Geohys. Res. Space Phys.* 121, 11364–11390. doi:10.1002/2016JA023119

Kane, R. P. (2005). Ionospheric <i>fo</i>F2 anomalies during some intense geomagnetic storms. *Ann. Geophys.* 23, 2487–2499. doi:10.5194/angeo-23-2487-2005

Kane, R. P. (1973a). Storm-time variations of F2. *Ann. Geophys.* 29, 25–42.

Kane, T. A., and Makarevich, R. A. (2010). HF radar observations of the F region ionospheric plasma response to Storm Sudden Commencements. *J. Geophys. Res. Space Phys.* 115, 1–13. doi:10.1029/2009ja014974

Karpachev, A. T., Klimenko, M. V., and Klimenko, V. V. (2019). Longitudinal variations of the ionospheric trough position. *Adv. Space Res.* 63, 950–966. doi:10.1016/j.asr.2018.09.038

Kouba, D., Boška, J., Galkin, I. A., Santolík, O., and šauli, P. (2008). Ionospheric drift measurements: Skymap points selection. *Radio Sci.* 43 (01), 1–11. doi:10.1029/2007RS003633

Kouba, D., and Koucká Knížová, P. (2012). Analysis of digisonde drift measurements quality. *J. Atmos. Solar-Terrestrial Phys.* 90-91, 212–221. doi:10.1016/j.jastp.2012.05.006

Kouba, D., and Koucká Knížová, P. (2016). Ionospheric vertical drift response at a mid-latitude station. *Adv. Space Res.* 58 (1), 108–116. doi:10.1016/j.asr.2016.04.018

Kumar, E. A., and Kumar, S. (2022). Geomagnetic storm effect on F2-region ionosphere during 2012 at low- and mid-latitude-latitude stations in the southern hemisphere. *Atmosphere* 13, 480. doi:10.3390/atmos13030480

Kumar, S., and Kumar, V. V. (2019). Ionospheric response to the St. Patrick's Day space weather events in March 2012, 2013, and 2015 at southern low and middle latitudes. *J. Geophys. Res. Space Phys.* 124, 584–602. doi:10.1029/2018JA025674

Lanzerotti, L. J., Cogger, L. L., and Mendillo, M. (1975). Latitude dependence of ionosphere total electron content: Observations during sudden commencement storms. *J. Geophys. Res.* 80 (10), 1287–1306. doi:10.1029/JA080i010p01287

Le Huy, M., and Amory-Mazaudier, C. (2008). Planetary magnetic signature of the storm wind disturbance dynamo currents:Ddyn. *J. Geophys.Res.* 113, A02312. doi:10.1029/2007JA012686

Li, W., Ma, Q., Thorne, R. M., Bortnik, J., Zhang, X., Li, J., et al. (2016). Radiation belt electron acceleration during the 17 March 2015 geomagnetic storm: Observations and simulations. *J. Geophys. Res. Space Phys.* 121, 5520–5536. doi:10.1002/2016JA022400

Liu, J., Wang, W., Burns, A., Yue, X., Zhang, S., Zhang, Y., et al. (2016). Profiles of ionospheric storm-enhanced density during the 17 March 2015 great storm. *J. Geophys. Res. Space Phys.* 121, 727–744. doi:10.1002/2015JA021832

Liu, L., Wan, W., Zhang, M.-L., Zhao, B., and Ning, B. (2008). Prestorm enhancements in NmF2 and total electron content at low latitudes. *J. Geophys. Res.* 113, A02311. doi:10.1029/2007JA012832

Liu, Y., and Xiong, C. (2020). Morphology evolution of the midlatitude ionospheric trough in nighttime under geomagnetic quiet conditions. *J. Geophys. Res. Space Phys.* 125, e2019JA027361. doi:10.1029/2019JA027361

Lu, G., Goncharenko, L., Nicolls, M. J., Maute, A., Coster, A., and Paxton, L. J. (2012). Ionospheric and thermospheric variations associated with prompt penetration electric fields. *J. Geophys. Res.* 117, A08312. doi:10.1029/2012JA017769

Lu, G., Zakharenkova, I., Cherniak, I., and Dang, T. (2020). Large-scale ionospheric disturbances during the 17 March 2015 storm: A model-data comparative study. *J. Geophys. Res. Space Phys.* 125, e2019JA027726. doi:10.1029/2019JA027726

Mansilla, G. A. (2003). Disturbances at F2-region heights of equatorial anomaly during geomagnetic storms. *J. Atmos. Solar-Terrestrial Phys.* 65 (9), 987–995. ISSN 1364-6826. doi:10.1016/S1364-6826(03)00119-6

Matsushita, S. (1959). A study of the morphology of ionospheric storms. *J. Geophys. Res.* 64, 305–321. doi:10.1029/jz064i003p00305

Mendillo, M., Klobuchar, J. A., and Hajeb-Hosseinieh, H. (1974). Ionospheric disturbances: Evidence for the contraction of the plasmasphere during severe geomagnetic storms. *Planet. Space Sci.* 22, 223–236. doi:10.1016/0032-0633(74)90026-9

Mendillo, M., and Narvaez, C. (2010). Ionospheric storms at geophysically-equivalent sites - Part 2: Local time storm patterns for sub-auroral ionospheres. *Ann. Geophys.* 28, 1449–1462. doi:10.5194/angeo-28-1449-2010

Mendillo, M., and Narvaez, C. (2009). Ionospheric storms at geophysically-equivalent sites – Part 1: Storm-time patterns for sub-auroral ionospheres. *Ann. Geophys* 27, 1679–1694. doi:10.5194/angeo-27-1679-2009

Mendillo, M. (2006). Storms in the ionosphere: Patterns and processes for total electron content. *Rev. Geophys.* 44, RG4001–47. doi:10.1029/2005rg000193

Mikhailov, A. V., and Forster, M. (1997). Day-to-day thermosphere parameter variation as deduced from Millstone Hill incoherent scatter radar observations during March 16–22, 1990 magnetic storm period. *Ann. Geophys.* 15, 1429–1438.

Mikhailov, A. V., and Perrone, L. (2009). Pre-storm NmF2 enhancements at middle latitudes: Delusion or reality? *Ann. Geophys* 27, 1321–1330. doi:10.5194/angeo-27-1321-2009

Mikhailov, A. V., Skoblin, M. G., and Forster, M. (1995). Daytime F2-layer positive storm effect at middle and lower latitudes. *Ann. Geophys.* 13, 532–540. doi:10.1007/s00585-995-0532-y

Mikhailov, A. V., Terekhin, Yu.L., and Mikhailov, V. V. (1989). Does the F2 layerfollow the constant pressure level? *Geomag. Aeron.* 29, 906–908.

Nava, B., Rodríguez-Zuluaga, J., Alazo-Cuartas, K., Kashcheyev, A., Migoya-Orué, Y., Radicella, S. M., et al. (2016). Middle- and low-latitude ionosphere response to 2015 St. Patrick's Day geomagnetic storm. *J. Geophys. Res. Space Phys.* 121, 3421–3438. doi:10.1002/2015ja022299

Nayak, C., Tsai, L.-C., Su, S.-Y., Galkin, I. A., Tan, A. T. K., Nofri, E., et al. (2016). Peculiar features of the low-latitude and midlatitude ionospheric response to the St. Patrick's Day geomagnetic storm of 17 March 2015. *J. Geophys. Res. Space Phys.* 121, 7941–7960. doi:10.1002/2016JA022489

Pirog, O. M., Polekh, N. M., Tashchilin, A. V., Romanova, E. B., and Zherebtsov, G. A. (2006). Response of ionosphere to the great geomagnetic storm of September 1998: Observation and modeling. *Adv. Space Res.* 37 (5), 1081–1087. doi:10.1016/j.asr.2006.02.005

Polekh, N., Zolotukhina, N., Kurkin, V., Zherebtsov, G., Shi, J., Wang, G., et al. (2017). Dynamics of ionospheric disturbances during the 17–19 March 2015 geomagnetic storm over East Asia. *Adv. Space Res.* 60 (11), 2464–2476. doi:10.1016/j.asr.2017.09.030

Prölss, G. W. (1995). "Ionospheric F-region storms," in *Handbook of atmospheric electrodynamics*. Editor H. Volland (Boca Raton, Fla: CRC Press).

Prölss, G. W., and Zahn, U. (1974). Esro 4 Gas Analyzer results 2. Direct measurements of changes in the neutral composition during an ionospheric storm. *J. Geophys. Res.* 79, 2535–2539. doi:10.1029/ja079i016p02535

Ram, S. T., Yokoyama, T., Otsuka, Y., Shiokawa, K., Sripathi, S., Veenadhari, B., et al. (2016). Duskside enhancement of equatorialzonal electric field response to convection electric fields during the St.Patrick's Day storm on 17 March 2015. *J. Geophys. Res. Space Phys.* 121, 538–548. doi:10.1002/2015ja021932

Ramsingh, T., Sripathi, S., Sreekumar, S., Banola, S., Emperumal, K., Tiwari, P., et al. (2015). Low-latitude ionosphere response tosuper geomagnetic storm of 17/18 March 2015: Results from a chain ofground-based observations over Indian sector. *J. Geophys. Res. SpacePhys.* 120, 10864–10882. doi:10.1002/2015JA021509

Ratovsky, K. G., Klimenko, M. V., Vasilyev, R. V., and Klimenko, V. V. (2019). "Upper atmosphere wind pattern during St. Patrick's day geomagnetic storm: Fabry-perot interferometer measurements and modeling," in 2019 PhotonIcs & Electromagnetics Research Symposium - Spring (PIERS-Spring), Italy, 17-20 June 2019.

Rishbeth, H., and Barron, D. W. (1960). Equilibrium electron distributions in the ionospheric F2-layer. *J. Atmos. Terr. Phys.* 18, 234–252. doi:10.1016/0021-9169(60)90095-7

Rodger, A. S., Brace, L. H., Hoegy, W. R., and Winningham, J. D. (1986). The poleward edge of the mid-latitude trough—its formation, orientation and dynamics. *J. Atmos. Terr. Phys.* 48, 715–728. doi:10.1016/0021-9169(86)90021-8

Rodger, A. S., Moffett, R. J., and Quegan, S. (1992). The role of ion drift in the formation of ionisation troughs in the mid- and high-latitude ionosphere—A review. *J. Atmos. Terr. Phys.* 54, 1–30. doi:10.1016/0021-9169(92)90082-v

Sato, T. (1957). Disturbances in the ionosphericF2 region asso-ciated with geomagnetic storms II. Middle latitudes. *J. Geomagn. Geoelectr.* 9, 1–22. doi:10.5636/jgg.9.1

Schunk, R. W., and Banks, P. M. (1975). Auroral N2 vibrational excitation and the electron density trough. *Geophys. Res. Lett.* 2, 239–242. doi:10.1029/gl002i006p00239

Seaton, M. J. (1956). A possible explanation of the drop in F-region criticaldensities accompanying major ionospheric storms. *J. Atmos. Terr.Phys.* 8, 122–124. doi:10.1016/0021-9169(56)90102-7

Tulasi, R. S., Yokoyama, T., Otsuka, Y., Shiokawa, K., Sripathi, S., Veenadhari, B., et al. (2016). Duskside enhance-ment of equatorial zonal electric field response to convection electricfields during the St. Patrick's Day storm on 17 March 2015. *J.Geophys. Res. Space Phys.* 121, 538–548. doi:10.1002/2015JA021932

Turunen, T., and Liszka, L. (1972). Comparison of simultaneous satellite measurements of auroral particle precipitation with bottomside ionosonde measurements of the electron density in the F-region. *J. Atmos. Terr. Phys.* 34, 365–372. doi:10.1016/0021-9169(72)90039-6

Voiculescu, M., Nygrn, T., Aikio, A., and Kuula, R. (2010). An olden but golden EISCAT observation of a quiet-time ionospheric trough. *J. Geophys. Res. Space Phys.* 115, 10315. doi:10.1029/2010JA015557

Voiculescu, M., Virtanen, I., and Nygrén, T. (2006). The F-region trough: Seasonal morphology and relation to interplanetary magnetic field. *Ann. Geophys.* 24, 173–185. doi:10.5194/angeo-24-173-2006

Werner, S., and Prölss, G. W. (1997). The position of the ionospheric trough as a function of local time and magnetic activity. *Adv. Space Res.* 20, 1717–1722. doi:10.1016/S0273-1177(97)00578-4

Whalen, J. A. (1989). The daytime F layer trough and its relation to ionospheric-magnetospheric convection. *J. Geophys. Res.* 94 (A12), 17169–17184. doi:10.1029/JA094iA12p17169

Wu, C. C., Liou, K., Lepping, R. P., Hutting, L., Plunkett, S., Howard, R. A., et al. (2016). The first super geomagnetic storm of solar cycle 24: "The St. Patrick's day event (17 March 2015)". *Earth Planet Sp.* 68, 151. doi:10.1186/s40623-016-0525-y

Yizengaw, E., Wei, H., Moldwin, M. B., Galvan, D., Mandrake, L., Mannucci, A., et al. (2005). The correlation between mid-latitude trough and the plasmapause. *Geophys. Res. Lett.* 32, L10102. doi:10.1029/2005GL022954

Zhang, J. J., Wang, C., Sun, T. R., Liu, C. M., and Wang, K. R. (2015). GIC due to storm sudden commencement in low-latitude high-voltage power network in China: Observation and simulation. *Space weather.* 13, 643–655. doi:10.1002/2015SW001263

Zhang, S. R., Erickson, P. J., Foster, J. C., Holt, J. M., Coster, A. J., Makela, J. J., et al. (2015). Thermospheric pole-ward wind surge at midlatitudes during great storm intervals. *Geophys.Res. Lett.* 42, 5132–5140. doi:10.1002/2015gl064836

Zhang, S. R., Erickson, P. J., Zhang, Y., Wang, W., Huang, C., Coster, A. J., et al. (2017a). Observations of ion-neutral coupling associated with strong electrodynamic disturbances during the 2015 St. Patrick's Day storm. *J. Geophys. Res. Space Phys.* 122, 1314–1337. doi:10.1002/2016JA023307

Zhang, S. R., Zhang, Y., Wang, W., and Verkhoglyadova, O. P. (2017b). Geospace system responses to the St. Patrick's Day storms in 2013 and 2015. *J. Geophys. Res. Space Phys.* 122, 6901–6906. doi:10.1002/2017JA024232